JACS
JOURNAL OF THE AMERICAN CHEMICAL SOCIETY

Article

pubs.acs.org/JACS

How Accurately Can Extended X-ray Absorption Spectra Be Predicted from First Principles? Implications for Modeling the Oxygen-Evolving Complex in Photosystem II

Martha A. Beckwith,[†,‡,▽] William Ames,[†,○] Fernando D. Vila,[§] Vera Krewald,[†] Dimitrios A. Pantazis,[†] Claire Mantel,[∥] Jacques Pécaut,[⊥] Marcello Gennari,[∥] Carole Duboc,[∥] Marie-Noëlle Collomb,[∥] Junko Yano,[#] John J. Rehr,[*,§] Frank Neese,[*,†] and Serena DeBeer[*,†,‡]

[†]Max Planck Institute for Chemical Energy Conversion, Stiftstraße 34-36, D-45470 Mülheim an der Ruhr, Germany

[‡]Department of Chemistry and Chemical Biology, Cornell University, Ithaca, New York 14853, United States

[§]Department of Physics, University of Washington, Seattle, Washington 98195, United States

[∥]Département de Chimie Moléculaire, Université Joseph Fourier Grenoble, CNRS, F-38000 Grenoble, France

[⊥]Laboratoire de Reconnaissance Ionique et Chimie de Coordination, Service de Chimie Inorganique et Biologique, (UMR E-3 CEA/UJF, FRE3200 CNRS), CEA-Grenoble, INAC, 17 rue des Martyrs 38054 Grenoble cedex 9, France

[#]Physical Biosciences Division, Lawrence Berkeley National Laboratory, Berkeley, California 94720, United States

Supporting Information

ABSTRACT: First principle calculations of extended X-ray absorption fine structure (EXAFS) data have seen widespread use in bioinorganic chemistry, perhaps most notably for modeling the Mn_4Ca site in the oxygen evolving complex (OEC) of photosystem II (PSII). The logic implied by the calculations rests on the assumption that it is possible to *a priori* predict an accurate EXAFS spectrum provided that the underlying geometric structure is correct. The present study investigates the extent to which this is possible using state of the art EXAFS theory. The FEFF program is used to evaluate the ability of a multiple scattering-based approach to directly calculate the EXAFS spectrum of crystallographically defined model complexes. The results of these parameter free predictions are compared with the more traditional approach of fitting FEFF calculated spectra to experimental data. A series of seven crystallographically characterized Mn monomers and dimers is used as a test set. The largest deviations between the FEFF calculated EXAFS spectra and the experimental EXAFS spectra arise from the amplitudes. The amplitude errors result from a combination of errors in calculated S_0^2 and Debye−Waller values as well as uncertainties in background subtraction. Additional errors may be attributed to structural parameters, particularly in cases where reliable high-resolution crystal structures are not available. Based on these investigations, the strengths and weaknesses of using first-principle EXAFS calculations as a predictive tool are discussed. We demonstrate that a range of DFT optimized structures of the OEC may all be considered consistent with experimental EXAFS data and that caution must be exercised when using EXAFS data to obtain topological arrangements of complex clusters.

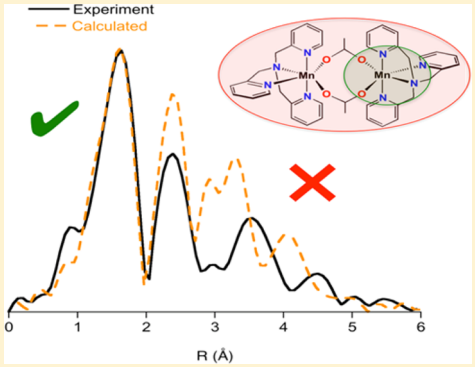

INTRODUCTION

X-ray absorption spectroscopy (XAS) is a powerful tool for determining the geometric and electronic structure of a transition-metal absorber. The extended X-ray absorption fine structure (EXAFS) region of the spectrum has had a particularly profound impact on our understanding of the local metrical structure of the transition-metal active sites in numerous metalloproteins. In many cases, EXAFS data have preceded the crystallographic characterization of proteins by years or even decades.[1,2] EXAFS data have also been utilized extensively to provide unique structural insights into enzymatic intermediates. Examples include characterization of the oxygen intermediates in methane monooxygenase,[3] ribonucleotide reductases,[4] P450s,[5] chloroperoxidases,[6] and multicopper oxidases[7] to name only a few. In the context of the present manuscript, we note that the current view of the Mn_4Ca cluster in photosystem II (PSII) has been greatly influenced by the results of detailed EXAFS studies. Most notably, more than three decades ago, Mn K-edge EXAFS studies first established the presence of a 2.7 Å Mn−Mn vector in the oxygen evolving complex (OEC) of photosystem II.[2] Numerous detailed EXAFS studies have followed, from which a general picture of the S-states in the OEC has emerged, with three (or two in the S_0 to S_2 states) short ∼2.7 Å Mn−Mn distances and one (or two in S_0 to S_3) long ∼3.3 Å Mn−Mn distances.[8−15] Using this metrical information, one would like to

Received: January 23, 2015
Published: September 9, 2015

DOI: 10.1021/jacs.5b00783
J. Am. Chem. Soc. 2015, 137, 12815−12834

reconstruct the three-dimensional structure which is consistent with these data. Interestingly, the EXAFS data have been used to argue for a wide range of highly varied topological models.[11,14,16−19]

Inherent in this discussion, is the question of how reliably can one predict EXAFS data based on multiple scattering calculations? Previous predictions by Yano, Batista, and most recently Pushkar utilized FEFF calculated EXAFS data, with either global Debye−Waller (DW) factors (in which the same DW value is used for all paths) or experimentally estimated DW factors (in which the DW values are fixed at values determined for known structures).[18−20] Yano et al. used fixed DW factors for the Mn−Mn and Mn−Ca vectors of PSII models based on previous fitting results from PSII and model compound studies, whereas Batista et al. and Pushkar used a global DW factor in the EXAFS calculations. Another approach that has been used by Ryde and co-workers is a combined DFT/EXAFS refinement procedure, in which either fixed DW factors[17] or FEFF calculated "equation of motion" DW are utilized.[16] The latter most closely parallels the $Calc_{DFT,CD}$ Method in the present study and has been applied to Ni and Cu model complexes, [Ni, Fe] hydrogenase, and most recently to the OEC.[16,21,22] However, a clear consensus picture on which three-dimensional structure(s) are most consistent with the EXAFS data has yet to emerge.

Clearly, if one intends to use the experimental EXAFS data in conjunction with calculations as a means to limit and define a three-dimensional structure in a system as complex as the OEC, one must first determine how reliably current state-of-the-art multiple scattering calculations are able to predict EXAFS of simple molecules based on their crystallographically determined structures. One should carefully differentiate between the fitting and prediction of EXAFS spectra. In the fitting approach a least-squares fit of DW factors and geometrical parameters in the EXAFS equation are varied until the best agreement with experiment is achieved. This approach has been used in countless successful studies, and when used properly, generally provides accurate metal−ligand distances. On the other hand, the prediction of EXAFS spectra implies that purely theoretical parameters are used in the EXAFS equation to obtain a spectrum to be compared to the experimental one. Thus, both the structure of the species under investigation as well as the DW and amplitude reduction factors need to be obtained on theoretical grounds. Only if it is possible to properly predict the EXAFS spectrum of molecules with known structure and known EXAFS spectra can this approach be used to judge the quality or plausibility of a theoretically obtained structure for an unknown system. To the best of our knowledge, the ability to use multiple scattering in the latter predictive way for complex molecular structures has never been rigorously assessed, despite its frequent use in application studies. The main purpose of this paper is to address this knowledge gap and assess how these results impact our understanding of the EXAFS for the OEC and more generally for all complex transition-metal-containing systems.

In order to address these questions, we have undertaken a systematic study of a series of monomeric and dimeric Mn model complexes, for which high accuracy small molecule crystal structures are known. First, FEFF is used to calculate phase and amplitude parameters, and then distances and DW values are refined, in a "standard" fitting approach. Then to test the ability to predict EXAFS, free of any refinement of parameters, FEFF is used to calculate the EXAFS based on the crystal structure using the correlated Debye (CD) model and also to calculate the EXAFS based on the DFT geometry optimized structure, using both the CD model and a more refined model, known as the dynamical matrix (DM) method, which uses harmonic frequencies obtained from DFT second derivatives.[23] Finally, a hybrid method is used in which the DM method is used to obtain DW values, and only distances are refined.

Using this information and comparing fit values to predicted values, we are able to assess which parameters from the FEFF calculations are most reliable and which require further refinement, either from experiment and/or computations. We then apply this approach to the S_1-state of the OEC and discuss the predicted EXAFS based on proposed literature models. We focus on the recently reported XFEL structure of Suga et al. at 1.95 Å resolution[24] and the 1.9 Å synchrotron XRD model of Umena et al.[25] As the latter is generally agreed to be radiation damaged, while the former is assumed to be damage free, these examples provide ideal limits for testing the robustness of the EXAFS data. Further, we go on to compare the predicted EXAFS to the experimental S_1-state data using previously proposed computational models by Siegbahn,[26] Batista,[27] and Pantazis et al.[28] We note that the Siegbahn S_1-state core is similar to QM/MM refined models, which were proposed later by both Batista[18] and Yamaguchi.[29,30] The broader implications for using EXAFS data in a predictive fashion are discussed.

EXPERIMENTAL SECTION

A set of three mononuclear and four binuclear manganese complexes was investigated (Scheme 1). The following abbreviations have been used for the ligands: terpy = 2,2′:6′,2″-terpyridine; phenylterpy = 4′-phenyl-2,2′:6′,2″-terpyridine; tpa = tris-2-picolylamine.

Synthesis of Complexes. The $[Mn(II)(tpa)Cl_2]$, $[Mn(II)(terpy)Cl_2]$, $[Mn(III)(phenylterpy)Cl_3]$, $[Mn_2(II)(\mu\text{-}OAc)_2(tpa)_2](PF_6)_2$, and $[Mn_2(III,IV)(\mu\text{-}O)_2(tpa)_2](PF_6)_3$ complexes were synthesized according to published procedures.[31−35] For $[Mn_2(III,IV)(\mu\text{-}O)_2(tpa)_2](PF_6)_3$, KPF_6 was used instead of $Na_2S_2O_6$.

Synthesis of $[Mn_2(III)(\mu\text{-}O)_2(tpa)_2](PF_6)_2$. This complex was prepared by an electrochemical procedure.[36,37] A solution of $[Mn_2(III,IV)(\mu\text{-}O)_2(tpa)_2](PF_6)_3$ (55 mg) in acetonitrile (6 mL) containing 0.1 M of $[Bu_4N]PF_6$ was reduced at −0.50 V vs $Ag/AgNO_3$ 10 mM under an argon atmosphere. Addition of diethyl ether to the solution after complete electrolysis (one electron exchanged per molecule of initial complex) led to the precipitation of $[Mn(III)(\mu\text{-}O)_2(tpa)_2](PF_6)_2$. The precipitate was filtered off, washed with diethyl ether, and dried under air (33 mg, yield 70%).

Synthesis of $[Mn_2(II)(\mu\text{-}SO_4)_2(tpa)_2]$. To a stirred solution of tpa (39.7 mg, 0.137 mmol) in 3 mL of methanol was added 7 mL of an aqueous solution of $Mn(SO_4)\cdot 2H_2O$ (23 mg, 0.137 mmol). The colorless solution was stirred for 30 min, filtered, and then evaporated to dryness to yield a white powder. White crystals of $[Mn_2(II)(\mu\text{-}SO_4)_2(tpa)_2]\cdot 3H_2O\cdot 2CH_3OH$ were grown by slow diffusion of diethyl ether in a concentrated solution of the white powder in methanol (30 mg, yield 24%). Elemental anal. calcd for $[Mn_2(II)(\mu\text{-}SO_4)_2(tpa)_2]\cdot 3H_2O$ ($C_{36}H_{36}Mn_2N_8O_8S_2\cdot 3H_2O$ (936)): C, 46.16; H, 4.52; N, 11.96; S, 6.84. Found: C, 45.92; H, 4.51; N, 11.84; S, 7.06. IR in cm^{-1} (KBr) n = 3455(s), 1602(s), 1573(m), 1557 (w), 1480(m), 1442(m), 1384 (w), 1354 (w), 1294 (m), 1191 (m), 1114(s), 1047 (m), 1015 (m), 911 (w), 773(m), 764 (m), 639 (w), 619(m), 514 (w), 412 (m). A full description of the crystal structure is given in the Supporting Information (Figure S1 and Tables S1 and S2). The CCDC reference number is CCDC 1024930.

Sample Preparation. All XAS samples were prepared as dilutions in boron nitride, pressed in Al spacers, and sealed with 38 μm Kapton windows. All samples were measured at 10 K in a liquid Helium cryostat.

XAS Data Collection. All XAS data were recorded at the Stanford Synchrotron Radiation Laboratory (SSRL) on focused beamline 9−3. A Si(220) monochromator was used for energy selection. A Rh-coated mirror (set to a cutoff of 10 keV) was used for harmonic rejection, in combination with 25% detuning of the monochromator. All data were

DOI: 10.1021/jacs.5b00783
J. Am. Chem. Soc. 2015, 137, 12815−12834

Scheme 1. Seven Manganese Complexes Investigated in This Study

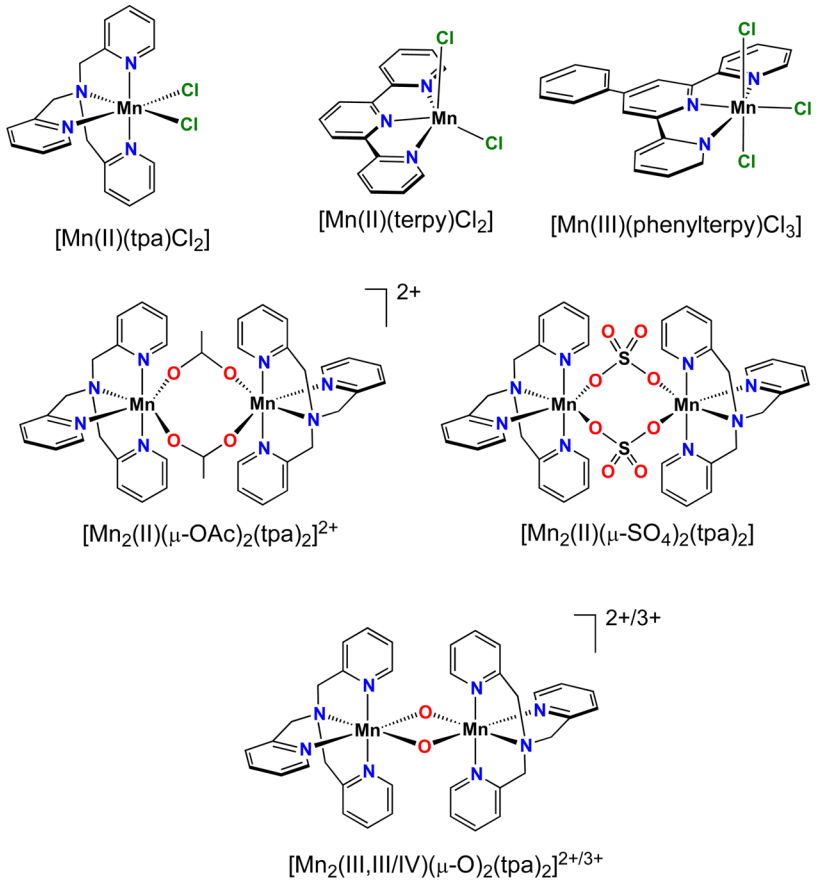

measured in transmission mode to $k = 12$ Å^{-1}, stopping at the Fe K-edge. Internal energy calibration was performed by simultaneous measurement of the absorption of a Mn foil placed between a second and third ionization chamber. The first inflection point of the Mn foil was assigned to 6539.0 eV. Samples were monitored for photoreduction throughout the course of data collection. Only those scans that showed no evidence of photoreduction were used in the final averages. The averaged data were processed as described previously.[38] A second-order polynomial was fit to the pre-edge region and subtracted from the entire spectrum. A three-region cubic spline was used to model the background above the edge using the program PySpline.[39]

EXAFS Calculations. Theoretical EXAFS spectra were calculated using both FEFF 7.0 and FEFF 9.1 which permits the inclusion of first-principle DW factors.[40,41] The EXAFS amplitude, $\chi(k)$, is given by[23]

$$\chi(k) = S_0^2 \sum_R N \frac{|f_{\text{eff}}(k)|}{kR^2} \sin(2kR + \phi_k) e^{-2kR/\lambda_k} e^{-2\sigma^2 k^2}$$

where S_0^2 is the overall many-body amplitude factor, N is the number of similar scatterers, $|f_{\text{eff}}(k)|$ is the effective scattering amplitude, R is the absorber−scatterer distance, $\exp(-2\sigma^2k^2)$ is a DW-like factor, λ_k is the mean free path of the photoelectron, and ϕ_k is the total phase shift for the photoelectron wave interaction with the absorber and the scatterer. All of the scattering paths contributing to the total EXAFS were calculated directly in FEFF using default parameters. The S_0^2 parameter was set to 1 for all calculations and fits except where noted. E_0 was fixed at 6550 eV, unless otherwise noted.

FEFF 7.0 Calculations. All calculations using FEFF 7 were performed using the following parameters: RMAX 5 (the effective path distance from the absorber), NLEG 3, CRITERIA 5 5. Hydrogen atoms were included in the calculations. Only 2- and 3-leg paths with $R < 5$ Å were calculated.

FEFF 9.1 Calculations. All calculations using FEFF 9 were performed using the following parameters: RPATH 5 (the effective path distance from absorber), NLEG 3, and CRITERIA 5 5. Presented spectra include hydrogen atoms for the Mn monomer and dimer complexes. We note that their exclusion did not alter the calculated spectra. Thus, for the OEC S1 model complexes hydrogen atoms were not included. Only 2- and 3-leg paths with $R < 5$ Å were calculated.

Five different approaches were examined for the EXAFS calculations:

Fit Method. Spectra were calculated with FEFF 7.0 using crystal structure coordinates,[31−35,42−44] and the resulting spectra were fit to the data using EXAFSPAK[45] as described previously.[38] The path distances, R, DW factors, σ^2, and the change in the edge energy, E_0, were allowed to refine during the fitting. The degeneracy values, N, were varied but were not allowed to refine. In order to reduce the number of free parameters, multiple scattering paths were grouped into related paths. This resulted in 11 fitted parameters for the monomers and 15 fitted parameters for the dimers. There are ∼22 degrees of freedom estimated for the present data. We note that for comparison, standard fits to OEC EXAFS employ 17−19 fitted parameters.[10]

The fits were performed in k-space ($k = 2$−11 Å^{-1} and $R = 0$−6 Å). Paths were added in subsequent fits until the reduced χ^2 error was minimized. The reduced χ^2 is defined in EXAFSPAK as $F/(\text{no. of points} - \text{no. of variables})$, where the normalized error F is given by

$$F = \sum_1^{N_T} \left(\frac{1}{s_i}\right)[\chi^{\text{expt}}(k_i) - \chi^{\text{calc}}(k_i)]^2$$

Here N_T is the total number of data points, $\chi^{\text{expt}}(k_i)$ is the experimental EXAFS amplitude at point i, and $\chi^{\text{calc}}(k_i)$ is the FEFF calculated EXAFS amplitude at point i. The normalization factor s_i is as follows:

$$\frac{1}{s_i} = \frac{k_i^3}{\sum_j^N k_j^3 |\chi^{\text{expt}}(k_j)|}$$

$\text{Calc}_{\text{XRD,CD}}$ Method. Spectra were calculated with FEFF 9.1 using crystal structure coordinates and the CD model.

DOI: 10.1021/jacs.5b00783
J. Am. Chem. Soc. 2015, 137, 12815−12834

$Calc_{DFT,CD}$ Method. Spectra were calculated with FEFF 9.1 using DFT geometry optimized structure coordinates and the CD model.

$Calc_{DFT,DM}$ Method. Spectra were calculated with FEFF 9.1 using DFT geometry optimized structure coordinates together with the DM model. Hessians were obtained from DFT frequency calculations, using the ORCA program,[46] as described below. In principle spectra can also be calculated using the DM model and the crystal structure coordinates. Results for a limited test set are presented in Figures S2−S4, and show generally similar trends. However, in some cases imaginary frequencies resulted, thus we have chosen to focus only on the DM model used in conjunction with the geometry optimized structures, for which no imaginary frequencies resulted.

$Calc_{DFT,DM\text{-}ref}$ Method. Spectra were calculated using the same approach as described in the $Calc_{DFT,DM}$ Method section, however distances were allowed to refine. This allows for a clearer assessment of the DW values obtained from the DM approach, given the refined metal−ligand bond lengths.

The differences between the two models used for calculating DW factors (i.e., the CD approach used in the $Calc_{XRD,CD}$ and $Calc_{DFT,CD}$ methods and the DM approach, used in the $Calc_{DFT,DM}$, and $Calc_{DFT,DM\text{-}ref}$ methods) are largely a result of the differences in how the vibrational density of states (VDOS) is calculated.

On the most sophisticated level ($Calc_{DFT,DM}$ and $Calc_{DFT,DM\text{-}ref}$ methods), the VDOS is calculated on the basis of the computed quantum chemical frequencies. We briefly outline the main points of the theory described in ref 23. To this end, the VDOS can be written in terms of the spectral resolution of the (mass weighted) Hessian matrix (usually called the "dynamical matrix" in the physics literature). In operator form, the VDOS operator takes the form:

$$\hat{\rho}(\omega) = -\frac{2\omega}{\pi}\sum_{k=1}^{3N_{At}-6(5)}\frac{|\mathbf{k}\rangle\langle\mathbf{k}|}{\omega^2 - d_k - i\varepsilon} \tag{1}$$

Here N_{At} is the number of atoms and hence $3N_{At} - 6(5)$ represents the number of vibrational degrees of freedom (5 for linear molecules), ω is the frequency, $|\mathbf{k}\rangle$ an eigenvector of the mass weighted Hessian matrix and d_k is its k'th eigenvalue (related to the harmonic frequency of the associated mode by $\omega_k = 1302.78\sqrt{d_k}$, in cm^{-1}). As usual, ε is a broadening parameter. The mass-weighted Hessian matrix is

$$\mathbf{D}_{KL} = \frac{1}{\sqrt{M_K M_L}}\frac{\partial^2 E}{\partial X_K \partial X_L} \tag{2}$$

Here X_K and X_L denote nuclear displacements and M_K and M_L are the masses of the atoms that belong to the given pair of displacements. Each scattering pathway **R** in a multiple scattering calculation consists of a number of atoms that build up the pathway. Let us denote the atoms and their associated displacements involved in a scattering pathway with $|\mathbf{Q}_R\rangle$ (this is a vector of length $3N_{At} - 6(5)$ that contains zeros for all atoms not involved in the pathway). One can then readily obtain a VDOS that is projected onto the given pathway as $\rho_R(\omega) = \mathrm{Im}\langle\mathbf{Q}_R|\hat{\rho}(\omega)|\mathbf{Q}_R\rangle$. This quantity essentially indicates how strongly a given scattering pathway contributes to the VDOS at a given frequency ω. Using this projected quantity and applying the reasoning outlined in the original references, the DW factor for a given pathway as a function of temperature is obtained by integrating over frequency to obtain:

$$\sigma_R^2(T) = \frac{\hbar}{2\mu_R}\int_0^\infty \frac{1}{\omega}\coth\left(\frac{\hbar\omega}{2k_B T}\right)\rho_R(\omega)d\omega \tag{3}$$

where μ_R is the reduced mass associated with the given scattering pathway **R** and k_B is Boltzmann's constant.

In the CD model (as applied for the $Calc_{XRD,CD}$ and $Calc_{DFT,CD}$ methods) a much simpler approach is taken.[47] Then the projected VDOS is approximated as

$$\rho_R(\omega) = \frac{3\omega^2}{w_D^3}\left[1 - \frac{\sin(\omega R/c)}{\omega R/c}\right] \tag{4}$$

where R is the absorber−scatterer path distance, w_D is the Debye cutoff frequency (the highest frequency that occurs in the system), $\theta_D = \hbar w_D/k_B$ is the Debye temperature, $c = w_D/k_D$ denotes the Debye approximation to the speed of sound, $k_D = (6\pi^2 N/V)^{1/3}$, and N/V is the atomic density number in the crystal.

As use of the CD model requires the Debye temperature as input, three different approaches were examined for estimating the Debye temperature. In the first approach, the sum of the first shell Mn−L stretching frequencies was used to determine the Debye temperature. The frequencies were determined by extracting quasidiatomic force constants from the numerical frequency calculations[48] (as described below). The second approach utilized the average of the Mn−L quasidiatomic force constants. This approach resulted in a dramatic underestimation of the FT amplitudes and hence is presented only in the Supporting Information (SI). Finally, a third approach was utilized in which a constant temperature of 1000 K was used for all model complexes. In most cases, this approach gave results reasonably similar to using the sum of the Mn−L stretching frequencies (see SI), with the advantage that input from DFT calculations are not required. Such an approach also more closely approximates the way EXAFS simulations are conventionally carried out.

Inclusion of Static Disorder. In order to facilitate the comparison of the FEFF calculated DW values ($Calc_{XRD,CD}$, $Calc_{DFT,CD}$, $Calc_{DFT,DM}$, and $Calc_{DFT,DM\text{-}ref}$ methods) to the fit DW values (Fit method), static disorder contributions must also be taken into account. Static disorder, in the present context, refers to multiple atoms being at effectively the same distance from the photoabsorber (within the resolution of an EXAFS measurement). For the present $k = 11$ Å^{-1} data, this corresponds to a ΔR of approximately 0.14 Å. This means that in the fits, two similar paths with Mn−L interactions <0.14 Å apart are grouped into a single path, which will have an average distance and a fit DW value, which includes both the thermal disorder for each path and the static disorder. Mathematically, the fit DW can thus be described as a sum of the thermal ($\sigma_R^2(T)$) and static disorder contributions $\sigma_R^2(sd)$, where

$$\sigma_R^2 = \sigma_R^2(T) + \sigma_R^2(sd) \tag{5}$$

$$\sigma_R^2(T) = \sum_i \frac{N_i}{N}\sigma_R^2(T) \tag{6}$$

$$\sigma_R^2(sd) = \sum_i (R_i - \langle R\rangle)^2\frac{N_i}{N} \tag{7}$$

Here $\langle R\rangle$ is the average distance for a given set of R_i distances. N_i corresponds to the numbers of times a given R_i path occurs (i.e., at the same exact distance), while N is the total number of occurrences of all R_i paths within the resolution of the data. For example, assume one has a Mn atom surrounded by three oxygens at 2.0, 2.1, and 2.1 Å, then $R_1 = 2.0$ Å, $N_1 = 1$, $R_2 = 2.1$ Å, $N_2 = 2$, $\langle R\rangle = 2.067$ Å and $N = 3$.

We note that without temperature-dependent measurements, the fit DW factors cannot be experimentally separated into the corresponding $\sigma_R^2(T)$ and $\sigma_R^2(sd)$ components. Thus, to compare our fit DW values (σ_R^2) to the theoretically calculated spectra, we have grouped the theoretically calculated paths by backscatterer identity and distance and calculated the theoretical σ_R^2 using eqs 5−7 above. Thus, all tabulated DW values correspond to both the thermal and static disorder contributions to each backscattering path. We note that for all predicted spectra the full atomic coordinates were used and the grouping into paths is only to facilitate comparison with the fits.

Electronic Structure Calculations. All quantum chemical calculations were carried out with the ORCA quantum chemistry package.[46] The molecular geometries of the Mn monomers were taken from the literature.[49] The molecular geometries of the Mn dimers were optimized using the BP86 functional.[50,51] Scalar relativistic effects were accounted for using ZORA,[52,53] and scalar relativistically recontracted versions of the all electron def2-TZVP basis sets were employed.[54−56] The conductor-like screening model[57] (COSMO) with $\varepsilon = 8$ and the zero-damping variant of the empirical dispersion correction by Grimme[58−60] (DFTD3 V1.3) to the DFT energy were used.

Frequencies were calculated at the same level of theory as the geometry optimizations. Inclusion of COSMO in the frequency calculations

DOI: 10.1021/jacs.5b00783
J. Am. Chem. Soc. 2015, 137, 12815−12834

did not significantly affect the theoretical EXAFS spectra in the subsequent FEFF calculations. The results presented include COSMO.

Six OEC models were investigated. Their core geometries are shown in Scheme 2, for a depiction of the full models see SI. Key distance parameters are provided in Table 1. Models **A** and **B** are the crystal structure coordinates taken from the 1.95 Å X-ray free electron laser structure and the 1.9 Å resolution crystal structure, respectively (PDB files with IDs 4UB8 and 3ARC).[24,25] Model **C** is taken from Siegbahn's optimized S_1 state model.[26] Model **D** is a cluster model adaptation by Siegbahn of an early QM/MM model by Batista.[27,61] Models **A**, **B**, **C** and **D** were taken directly from the literature, i.e., no geometry optimizations were performed. Models **E** and **F** contain the Mn and O coordinates from the polarized EXAFS cores II and III, respectively, in the ligand surrounding from a study of Pantazis and co-workers (labeled 2 and 6 in the original study).[14,28]

To improve comparability of the models, they were truncated to approximately the same size. They include only first-coordination sphere residues of the Mn and Ca ions and selected crystallographic water molecules (see SI). Note that the geometries of **C** and **D** are models of the S_1 state, and also the cores of models **E** and **F** are the cores inferred based on the single crystal EXAFS experiments of the S_1 state.[14] The XFEL model **A** represents the first putatively damage free three-dimensional structure of the S_1 state. On the other hand, the XRD model **B** is generally agreed to be radiation damaged and likely corresponds to a state or mixture of states that is not directly relevant to the catalytic cycle.[10,11,62,63]

Scheme 2. Cores of the OEC Models Used Here[a]

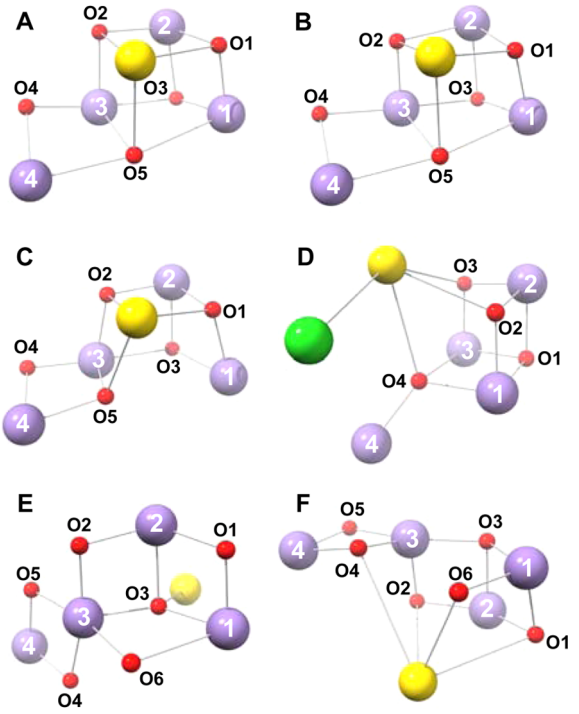

[a]Color scheme: Mn, purple; Ca, yellow; Cl, green; O, red.

Table 1. Relevant Distance Parameters (in Å) for the OEC Model Complexes Shown in Scheme 2

model	A	B	C	D	E	F
Mn1−Mn2	2.74	2.84	2.83	2.78	2.8	2.80
Mn1−Mn3	3.27	3.29	3.43	2.92	3.28	3.25
Mn1−Mn4	4.97	5.00	5.07	3.23	5.49	5.46
Mn2−Mn3	2.73	2.89	2.81	2.78	2.7	2.72
Mn2−Mn4	5.21	5.44	5.14	5.25	4.96	4.97
Mn3−Mn4	2.88	2.97	2.76	3.67	2.72	2.72
Mn1−Ca	3.49	3.51	3.73	3.71	3.41	3.40
Mn2−Ca	3.33	3.36	3.45	3.38	3.41	3.40
Mn3−Ca	3.41	3.41	3.62	3.8	3.75	3.73
Mn4−Ca	3.71	3.79	3.78	4.17	4.41	4.38
Mn1−O	1.81	1.87	1.89	1.89	1.86	1.88
Mn1−O	1.80	1.81	1.96	1.81	1.89	1.94
Mn1−O		2.60		1.89		
Mn2−O	1.88	2.06	1.82	1.90	1.86	1.85
Mn2−O	1.83	2.13	1.78	1.79	1.82	1.82
Mn2−O	2.01	2.10	1.89	1.79	2.02	1.91
Mn3−O	2.00	1.87	1.86	1.92	1.78	1.81
Mn3−O	2.14	2.13	2.10	1.84	1.85	1.87
Mn3−O	1.89	2.09	1.76	2.43	1.92	1.77
Mn3−O	2.32	2.38	1.79		1.87	1.80
Mn4−O	2.05	2.11	1.90	1.86	1.76	1.81
Mn4−O	2.38	2.50	1.95		1.76	1.74

RESULTS AND DISCUSSION

Fits to the Mn Monomers EXAFS Data. Figure 1 shows the experimental data and the fits to the data for the Mn monomers. The fits were obtained by first calculating the $\chi(k)$ spectra using FEFF 7.0 and then allowing the distances, σ^2 values, and ΔE_0 to refine. The metrical parameters are summarized in Table 2, column 1. These results, not surprisingly, show excellent agreement with the experimental EXAFS, with error values (reduced χ^2) ranging from 0.31 to 0.80 over the series of monomers. As may be expected, a further decrease in the χ^2 value results when S_0^2 is allowed to refine. We note however that by increasing the number of free parameters, one also risks overfitting the EXAFS data. This in fact is one of the primary motivations toward improving the predictive capability of EXAFS calculations. Regardless, the distances obtained in the present study (Table 2) are in reasonable agreement with the crystallographic distances, with first shell Mn−Cl distances deviating by <0.02 Å from the crystallographic values. A slightly larger error is seen for the Mn−N distances, with deviations of 0.03−0.06 Å, relative to the crystal structure. A larger error in light atom interactions (i.e., N) is generally expected in the presence of a heavier scatterer (i.e., Cl). As there are numerous paths, which contribute to the Mn−C and Mn−C−N paths because of the larger number of C atoms in the terpy ligand (Figure S5), a direct comparison with the crystal structure is more difficult to assess for these particular path contributions. On the other hand, it should be emphasized that some of the fitted DW factors may be unphysical since they are correlated with amplitude factors and differ significantly from the calculated values. However, the Mn−C−N multiple scattering paths do not have a significant contribution to the total EXAFS (FT magnitudes on the order of ∼0.06 compared to ∼2.0 in the first shell of the experimental FT). In any case, visual inspection of the data and the fit in both EXAFS and FT shows good agreement. This approach to analyzing EXAFS data is, of course, the most common approach used in the literature. It, however, fails to illustrate the difference between the data and first-principles calculations, which is essential if one wishes to use EXAFS calculations in a predictive fashion. In order to better assess this, we present the FEFF calculated spectra below.

FEFF Calculated EXAFS Spectra for the Mn Monomers: $Calc_{XRD,CD}$, $Calc_{DFT,CD}$, and $Calc_{DFT,DM}$ Methods. Figure 2 presents the direct FEFF calculated spectra using the $Calc_{XRD,CD}$, $Calc_{DFT,CD}$, and $Calc_{DFT,DM}$ methods without any fitting of parameters. These results are summarized in Table 2, columns 2−4,

DOI: 10.1021/jacs.5b00783
J. Am. Chem. Soc. 2015, 137, 12815−12834

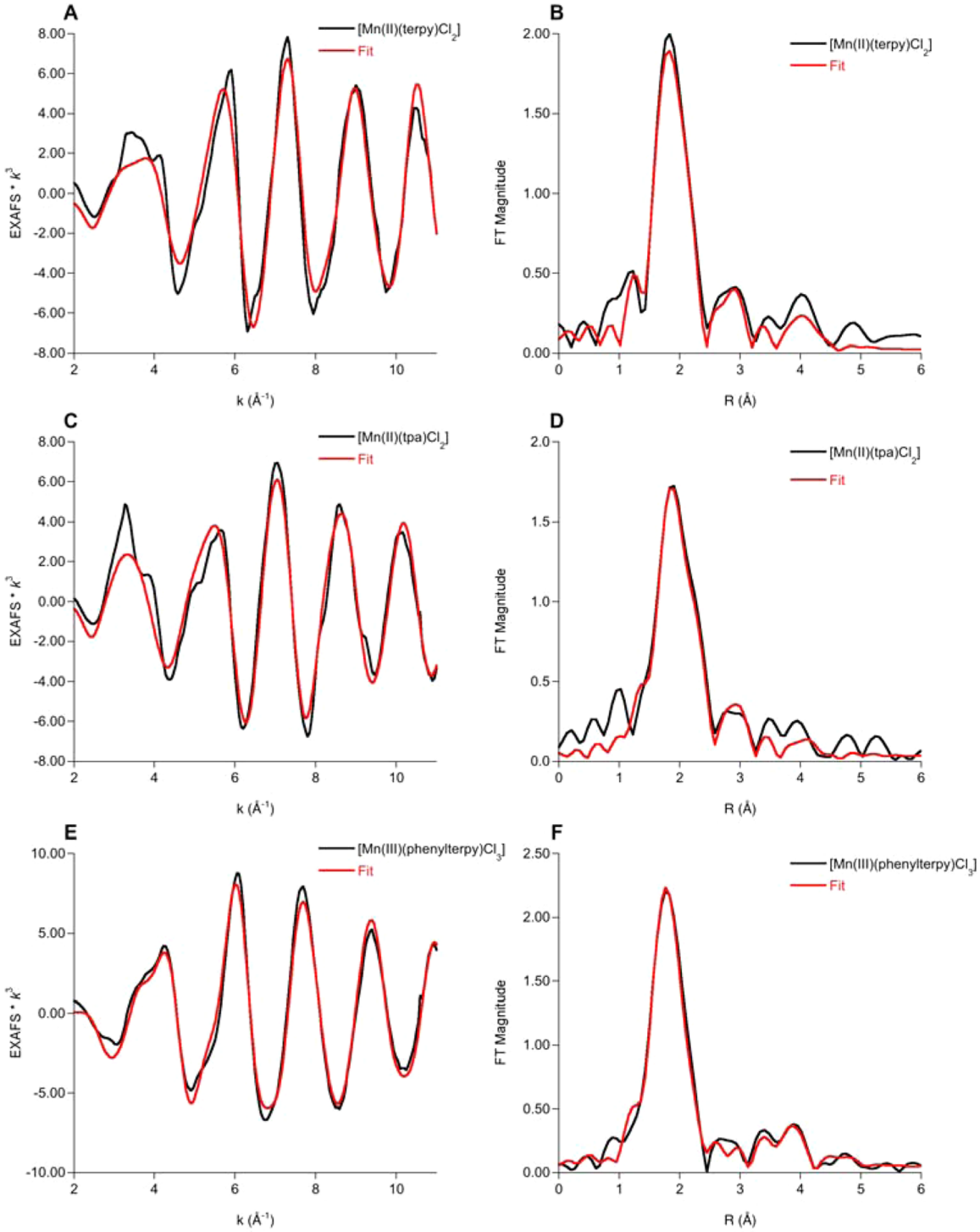

Figure 1. Experimental (black) and fits (red) to the $\chi(k)$ spectra and the corresponding non-phase shift corrected FTs of $[Mn(II)(terpy)Cl_2]$ (A and B), $[Mn(II)(tpa)Cl_2]$ (C and D), and $[Mn(III)(phenylterpy)Cl_3]$ (E and F).

and Figure 2. In addition, to account for amplitude errors resulting from uncertainties in background subtraction, a second set of fits was performed for each method in which S_0^2 was allowed to refine. For all of the monomers, the S_0^2 values refined to values between 0.7 and 0.9 for methods 2−4. These fits are presented in the Figure S12, and the corresponding χ^2 value is given in Table 2. While all of the theoretical spectra reproduce the general shape of the experimental spectra reasonably well in the first shell (i.e., at distances, R, between 0 and 2.5 Å), there are discrepancies in the calculated intensity and in the distributions and intensity of the outer shell features (R > 2.5 Å) relative to experiment (Figure 2). We note that these discrepancies remain, even when S_0^2 is allowed to refine (Figure S12). Not surprisingly, without fitting the calculated spectra to the experimental data, one observes a substantial increase in the error values, by a factor of up to ∼7 (Table 2), which is also observed visually in the calculated spectra (Figure 2). Here we more closely evaluate the origin of these differences in each computational approach.

$Calc_{XRD,CD}$ Method. It is perhaps most instructive to first compare the $Calc_{XRD,CD}$ method calculated spectra to the fit data,

DOI: 10.1021/jacs.5b00783
J. Am. Chem. Soc. 2015, 137, 12815−12834

Table 2. Comparison of Path Distances and DW Factors of the Mn Monomer Fits to Those Calculated from the Crystal Structures Using the CD Method in FEFF 9.1 and from the Geometry Optimized Structures Using Both the CD Method in FEFF 9.1, and the DM Method in FEFF 9.1 with and without Distance Refinement[a]

path		fit	$Calc_{XRD,CD}$	$Calc_{DFT,CD}$	$Calc_{DFT,DM}$	$Calc_{DFT,DM\text{-}ref}$
		[Mn(II)(terpy)Cl_2]				
Mn−N	R (Å)	2.21 (±0.0098)	2.24	2.24	2.24	2.26
	σ^2 (Å^2)	0.0044 (±0.0012)	0.0038	0.0046	0.0040	0.0040
Mn−Cl	R (Å)	2.36 (±0.0038)	2.36	2.34	2.34	2.35
	σ^2 (Å^2)	0.0025 (±0.0005)	0.0017	0.0020	0.0028	0.0028
Mn−C[b]	R (Å)	3.13 (±0.0104), 4.62 (±0.0143)	3.14, 4.48	3.14, 4.47	3.14, 4.47	3.11, 4.67
	σ^2 (Å^2)	0.0061 (±0.0012), 0.0034 (±0.0015)	0.0061, 0.0052	0.0065, 0.0060	0.0054, 0.0051	0.0054, 0.0051
Mn−C−N	R (Å)	3.26 (±0.0256)	3.37	3.36	3.36	3.31
	σ^2 (Å^2)	0.0052 (±0.0045)	0.0048	0.0056	0.0043	0.0043
error (reduced χ^2)[c]		0.803	1.75	2.70	2.59	0.788
refined S_0^2		1.006	0.791	0.769	0.791	0.987
error (S_0^2 refined)		0.772	1.23	2.11	2.13	0.772
		[Mn(II)(tpa)Cl_2]				
Mn−N	R (Å)	2.27 (±0.0082)	2.33	2.33	2.33	2.30
	σ^2 (Å^2)	0.0067 (±0.0010)	0.0052	0.0087	0.0080	0.0080
Mn−Cl	R (Å)	2.44 (±0.0033)	2.44	2.43	2.43	2.42
	σ^2 (Å^2)	0.0025 (±0.0004)	0.0019	0.0039	0.0051	0.0051
Mn−C[b]	R (Å)	3.15 (±0.0094), 4.68 (±0.0256)	3.19, 4.53	3.19, 4.53	3.19, 4.53	3.16, 4.73
	σ^2 (Å^2)	0.0026 (±0.0012), 0.0075 (±0.0030)	0.0094, 0.0066	0.0100, 0.0080	0.0089, 0.0069	0.0089, 0.0069
Mn−C−N	R (Å)	3.44 (±0.0147)	3.46	3.46	3.46	3.42
	σ^2 (Å^2)	0.0015 (±0.0019)	0.0070	0.0100	0.0085	0.0085
error (reduced χ^2)		0.585	2.13	1.94	2.23	0.917
refined S_0^2		0.998	0.730	0.874	0.876	1.041
error (S_0^2 refined)		0.562	1.31	1.83	2.14	0.889
		[Mn(III)(phenylterpy)Cl_3]				
Mn−N	R (Å)	2.13 (±0.0066)	2.17	2.21	2.21	2.40
	σ^2 (Å^2)	0.0062 (±0.0010)	0.0070	0.0073	0.0074	0.0074
Mn−Cl	R (Å)	2.29 (±0.0027)	2.27	2.29	2.29	2.24
	σ^2 (Å^2)	0.0049 (±0.0003)	0.0019	0.0017	0.0028	0.0028
Mn−C	R (Å)	2.90 (±0.0186)	3.07	3.11	3.11	3.49
	σ^2 (Å^2)	0.0018 (±0.0024)	0.0063	0.0072	0.0071	0.0071
Mn−C−N[b]	R (Å)	4.51 (±0.0080), 5.06 (±0.0115)	4.47, 4.96	4.48, 4.64	4.48, 4.64	4.76, 4.82
	σ^2 (Å^2)	0.0015 (±0.0008), 0.0010 (±0.0015)	0.0086, 0.0063	0.0087, 0.0046	0.0083, 0.0043	0.0083, 0.0043
error (reduced χ^2)		0.313	2.15	2.25	1.56	1.19
refined S_0^2		0.999	0.716	0.763	0.861	0.924
error (S_0^2 refined)		0.301	0.610	1.38	1.33	1.10

[a]All distances and DW factors shown are the average values for each scattering path. Standard deviations for the fit values are given in parentheses. [b]Two paths of this type were included in the fit to the data. The corresponding distances and DW factors are separated by commas. [c]A measure of the error value between the experimental data and the EXAFS calculated via each method, where reduced $\chi^2 = F/(\text{no. of points} - \text{no. of variables})$ and $F = \Sigma_i\, [k_i^3/(\Sigma_j\, k_j^3\, |\chi^{expt}(k_j)|)]^2[\chi^{expt}(k_i) - \chi^{calc}(k_i)]^2$. In the case of the fit the error is between the data and the final fit to the data.

as this approach uses the crystallographic coordinates. Table 2 (columns 1 and 2) highlights the differences between the crystal structure and the fit EXAFS data. For all three monomers, the error value has increased significantly, with the largest deviation occurring for the complex [Mn(III)(phenylterpy)Cl_3]. As noted above, the first shell Mn−Cl distances are in very good agreement with the EXAFS fit distances. However, larger differences are observed for the more weakly scattering Mn−N distances as well as the outer shell Mn−C distances. The differences between the $Calc_{XRD,CD}$ method and the fit data are summarized in Table 3, column 1. The differences between the fit and calculated distances and DW factors are reported, together with scaling factors by which the calculated values are multiplied to give the fit values (for the fits where $S_0^2 = 1$). We note that by keeping S_0^2 fixed, the apparent contribution of the DW to the amplitude error is maximized. However, as the S_0^2 values were also fixed in the fitting procedure, this allows for the most straightforward comparison of these values. As an example, the Mn−N distance from the [Mn(II)(terpy)Cl_2] crystal structure, 2.24 Å, is 0.03 Å longer than the fit distance of 2.21 Å, thus corresponding to a scaling factor of ∼0.98 between the calculated and fit distances. Over the series of monomers, the scaling factor in the calculated and fit distances for the first shell paths ranges from ∼0.97−1.01. Similar trends are observed for the longer distance single and multiple scattering paths involving atoms that are part of the terpy or tpa ligands (Mn−C and Mn−C−N), though the scaling factors between the calculated and fit distances span a slightly larger range (ΔR = ∼ 0.94−1.03). This may be attributed to the larger number of paths that comprise the 2.5−5.0 Å region of the FT.

While the calculated distance values are reasonably similar to the fit distances, this is not the case for the DW factors. Using the $Calc_{XRD,CD}$ method, the average calculated DW factors (Table 2) differ from the fit DW factors by scaling factors of ∼0.89−2.63 for

DOI: 10.1021/jacs.5b00783
J. Am. Chem. Soc. 2015, 137, 12815−12834

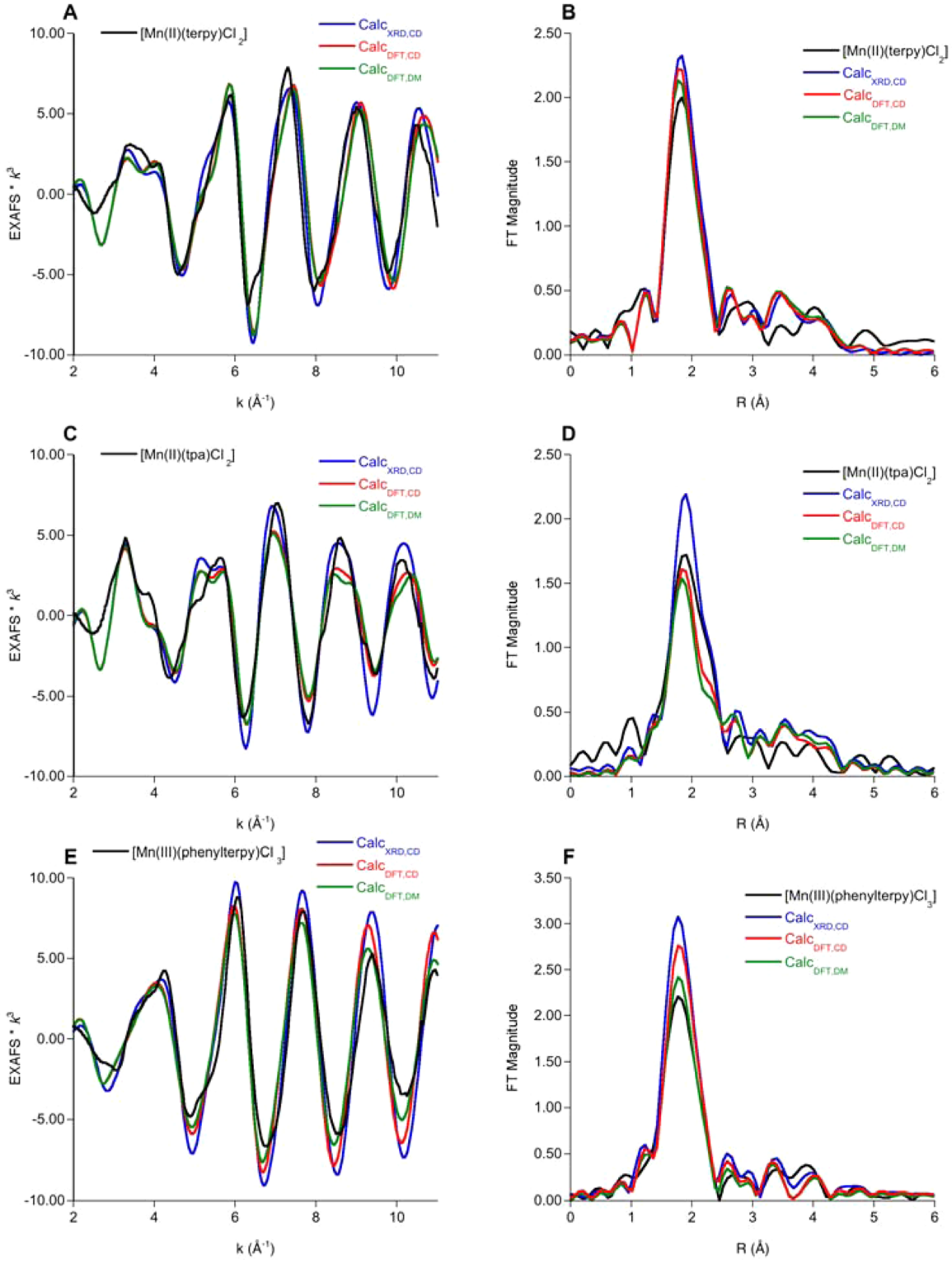

Figure 2. Experimental (black) and theoretical $\chi(k)$ spectra calculated using FEFF 9.1 and the corresponding non-phase shift corrected FTs of [Mn(II)(terpy)Cl_2] (A and B), [Mn(II)(tpa)Cl_2] (C and D), and [Mn(III)(phenylterpy)Cl_3] (E and F). The calculations for the spectra using the $Calc_{DFT,CD}$ method included Debye temperatures determined using the sum of the first shell Mn−L stretching frequencies.

the first shell paths (0 Å < R < 2.5 Å), and by scaling factors ∼0.16−1.13 for the outer shell paths (i.e., contributions at R > 2.5 Å).

We note that the full range of outer shell paths is not reported in Table 3. Table 3 reports only the single scattering contributions. Multiple scattering contributions are on average found to have even larger deviations between the calculated vs fit DW values.

Again, we emphasize that the large apparent deviations in the DW values derive in part from the approach we are using to compare the fit to the calculations. Since in the fixed S_0^2 fits, only the DW values were refined, the comparison necessarily accounts

DOI: 10.1021/jacs.5b00783
J. Am. Chem. Soc. 2015, 137, 12815−12834

Table 3. Differences between the Final Fit Parameters and the FEFF 9.1 Calculated Parameters for the Mn Monomers, Using the $Calc_{XRD,CD}$, $Calc_{DFT,CD}$, $Calc_{DFT,DM}$, and $Calc_{DFT,DM\text{-}ref}$ Methods[a]

path		$Calc_{XRD,CD}$ (absolute deviation)	$Calc_{XRD,CD}$ (scaling factor)	$Calc_{DFT,CD}$ (absolute deviation)	$Calc_{DFT,CD}$ (scaling factor)	$Calc_{DFT,DM}$ (absolute deviation)	$Calc_{DFT,DM}$ (scaling factor)	$Calc_{DFT,DM\text{-}ref}$ (absolute deviation)	$Calc_{DFT,DM\text{-}ref}$ (scaling factor)
Mn−Cl 2.3−2.4 Å	ΔR (Å)	−0.02 to 0	1.00 to 1.01	−0.02 to 0	1.00 to 1.01	−0.02 to 0	1.00 to 1.01	−0.05 to −0.01	1.00 to 1.02
	$\Delta\sigma^2$ (Å^2)	−0.0030 to −0.0006	1.30 to 2.63	−0.0032 to +0.0014	0.64 to 2.89	−0.0021 to +0.0026	0.49 to 1.76	−0.0021 to +0.0026	0.49 to 1.76
Mn−N 2.1−2.3 Å	ΔR (Å)	+0.03 to +0.06	0.97 to 0.98	+0.03 to +0.08	0.96 to 0.99	+0.03 to +0.08	0.96 to 0.99	+0.03 to +0.3	0.89 to 0.99
	$\Delta\sigma^2$ (Å^2)	−0.0015 to +0.0008	0.89 to 1.29	+0.0002 to +0.0020	0.77 to 0.95	−0.0004 to +0.0013	0.84 to 1.11	−0.0004 to +0.0013	0.84 to 1.11
Mn−C 2.9−3.2 Å	ΔR (Å)	+0.01 to +0.17	0.94 to 1.00	+0.01 to +0.21	0.93 to 1.00	+0.01 to +0.21	0.93 to 1.00	−0.02 to +0.6	0.83 to 1.01
	$\Delta\sigma^2$ (Å^2)	0 to +0.0068	0.28 to 1.00	+0.0004 to +0.0074	0.25 to 0.94	−0.0007 to +0.0063	0.25 to 1.12	−0.0007 to +0.0063	0.25 to 1.12

[a]Values have been obtained by subtracting the averaged fit values for a given path from the averaged calculated values for a given path. The scaling factor is the value by which the FEFF calculated parameter is multiplied in order to obtain the fit parameter (i.e. fit parameter = calculated parameter × scaling factor). We note that the deviation in the DW values also reflects other contributions to the amplitude errors (including S_0^2 and the background subtraction).

for all of the amplitude error in the deviation of the DW. We emphasize that these differences more generally reflect overall amplitude errors, which will have contributions not only from the DW values but also from S_0^2 and the background subtraction. Importantly, this comparison is intended to emphasize that significant deviations exist between the predicted and experimental spectra, and the deviation arises in part from differences in the amplitudes.

$Calc_{DFT,CD}$ Method. In addition to using the crystallographic coordinates ($Calc_{XRD,CD}$ method), we also tested the FEFF 9.1 CD model using DFT geometry optimized structures ($Calc_{DFT,CD}$ method). The results of these calculations are summarized in Figure 2 and Tables 1 and 2. As can be clearly seen in Table 2, the geometry optimized distances are quite similar to the crystallographic distances, with deviations of 0.01−0.02 Å in the first shell distances and somewhat larger deviations in the outer shell contributions. Overall the root-mean-square deviations, excluding hydrogen atoms, between the crystallographic coordinates and the geometry optimized structures range from 0.247 to 0.922, indicating generally reasonable agreement. As the changes in distances are relatively small, it is perhaps not surprising that there is correspondingly essentially no change in the DW values between the $Calc_{XRD,CD}$ and $Calc_{DFT,CD}$ methods (Table 2).

The small changes in FT intensities between the $Calc_{XRD,CD}$ and $Calc_{DFT,CD}$ methods (see Figure 2D,F) reflect the slight differences in bond length distribution rather than differences in the calculated disorder parameters. This is more clearly illustrated by examining the deconvolution of the calculated spectrum of [Mn(II)(tpa)Cl_2] as presented in Figure 3. There are noticeable differences in the intensities of the individual components using the $Calc_{XRD,CD}$ and $Calc_{DFT,CD}$ methods, particularly for the Mn−Cl and Mn−N contributions. This originates from a larger distribution in the Mn−Cl and Mn−N distances in the geometry optimized structure, as compared to the crystal structure. We note that in the crystal structure the Mn−Cl distances are 2.42 and 2.45 Å, while in the geometry optimized structure the Mn−Cl vectors are 2.39 and 2.47 Å. Similarly for the Mn−N distances the experimental vectors of 2.29, 2.29, 2.35, and 2.40 Å show a somewhat larger distribution in the geometry optimized structure, with values of 2.26, 2.27, 2.38, and 2.41 Å, respectively. This results in a higher calculated total first shell FT intensity for the $Calc_{XRD,CD}$ method than for the $Calc_{DFT,CD}$ method (a total FT magnitude of 2.2 vs 1.8, Figure 2D). This further highlights the importance of having both accurate distances and DW values in order to make spectral predictions.

$Calc_{DFT,DM}$ Method. As the correlated Debye model did not produce satisfactory results at either the crystallographic coordinates or at the geometry optimized structures, in part due to errors in the DW values, we explored an alternate method for obtaining these values. DFT frequencies were used within the FEFF DMDW code in order to obtain the values for mean bond displacements. These results are summarized in Figure 2 and Tables 1 and 2 (last column).

By inspection of Figure 2 and Table 2, one can see that in certain cases, the $Calc_{DFT,DM}$ method gives slightly better predicted spectra ([Mn(III)(phenylterpy)Cl_3]), while in other cases, it is slightly worse. Specifically, for the geometry optimized structure of [Mn(II)(tpa)Cl_2], the DW value for the Mn−Cl path calculated using the DM method is almost 50% larger than the DW value calculated using the CD method ($Calc_{DFT,CD}$) at the same structure (Table 2). This larger DW value results in a decrease in the intensity of the FT for this path (Figure 3). As the Mn−Cl path dominates the first shell FT spectral intensity, this results in a total calculated first shell FT intensity that is too low. In general, the DW factors calculated using the $Calc_{DFT,DM}$ method differ from the fit values by scaling factors of 0.49−1.76 for the first shell paths and by scaling factors of 0.18−1.22 for outer shell paths (as with the $Calc_{XRD,CD}$ and $Calc_{DFT,CD}$ methods, the scaling factors for the multiple scattering paths are not reported in Table 3). These differences are generally lower than those for the $Calc_{XRD,CD}$ and $Calc_{DFT,CD}$ methods (first shell 0.89−2.63, outer shell 0.16−1.13), indicating that the $Calc_{DFT,DM}$ method results in slightly better calculated DW values than either the $Calc_{XRD,CD}$ method or the $Calc_{DFT,CD}$ method, particularly in the first shell. However, given that the direct calculation of the DW factors through quantum chemically calculated frequencies represents much more rigorous physics than the simple CD model (which amounts to a spherical approximation), the result is still somewhat disappointing. In particular because quantum chemical frequencies from DFT calculations are well-known to be quite precise in the overwhelming majority of cases.[64,65]

FEFF Calculated EXAFS Spectra with Fit Distances for the Mn Monomers: $Calc_{DFT,DM\text{-}ref}$ Method. A final approach

DOI: 10.1021/jacs.5b00783
J. Am. Chem. Soc. 2015, 137, 12815−12834

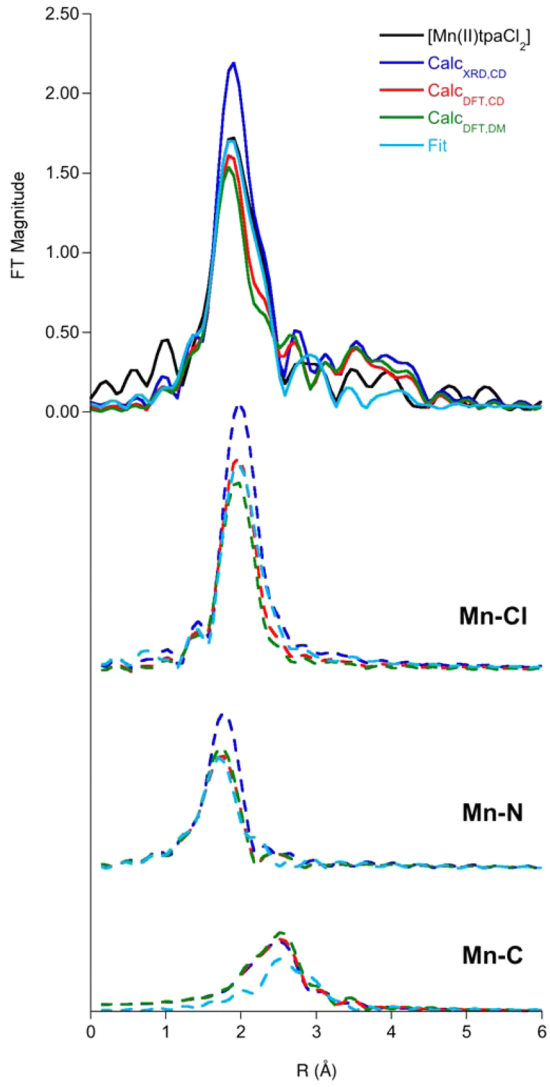

Figure 3. Calculated spectra and contributions of significant single scattering paths to the total spectra for [Mn(II)(tpa)Cl_2]. The deconvolutions for each method are the sums of the individual scattering paths of each type. The calculations for the spectra using the $Calc_{DFT,CD}$ method included Debye temperatures determined using the sum of the first shell Mn−L stretching frequencies. Spectra have been offset on the *y*-axis, but share a common *y*-scale.

was taken in which the $Calc_{DFT,DM}$ DMDW calculated DW values were used in combination with fit distances ($Calc_{DFT,DM-ref}$ method, Table 2 and SI). In all cases the error value is lower than that obtained for the purely theoretical spectra. And in one case, [Mn(II)(terpy)Cl_2], the error using the $Calc_{DFT,DM-ref}$ method is as low as that of the fit, however, with far fewer free parameters. We also note, however, that by fixing the DW values too far from the fit minimum, the partial fit compensates by refining the distances to values quite far from the crystallographic or geometry optimized structures. This can be most clearly seen when comparing the fit and $Calc_{DFT,DM-ref}$ method results for [Mn(III)(phenylterpy)Cl_3]. In the $Calc_{DFT,DM-ref}$ method, the Mn−N DW is fixed at a value that is too large (relative to the fit value), while the Mn−Cl DW is fixed at a value that is too small. As a result the Mn−N bond length shifts to a longer distance (by 0.23 Å), while the Mn−Cl bond shifts to a shorter distance (by 0.05 Å). These are large deviations relative to both the fit and the crystallographically determined distances and indicate that fixing the DW while refining the distances can result in unreasonable minima. It also demonstrates that the DMDW derived DW values can deviate greatly from the fit values and that this deviation is not uniform (i.e., the values may be either under or overestimated). Nevertheless, the results from this partial fit highlight the effect of the structural differences. The marked improvement in the χ^2 when the structural parameters are allowed to refine shows that differences between the theoretical and fit structures also plays an important a role in determining the agreement between the theoretical and experimental EXAFS. While in this particular test set, the deviations in the refined distances are well outside the error limits of small molecule crystallography, such structural differences clearly can play an important role when a crystal structure is not available or when the error in the structure may be large (as is often the case in protein crystallography). Nonetheless, the difference in the structural parameters associated with these models should be taken as a cautionary tale when assigning structures based solely on the agreement between theoretical and measured EXAFS spectra.

The Impact of S_0^2 Values on the Predicted Mn Monomer Spectra. As noted above, for the $Calc_{XRD,CD}$, $Calc_{DFT,CD}$, $Calc_{DFT,DM}$, and $Calc_{DFT,DM-ref}$ methods, one can also improve agreement with the experimental data by refining the amplitude parameter, S_0^2. Specifically for the $Calc_{XRD,CD}$ method, by allowing S_0^2 to decrease to a value between 0.7 and 0.8, better agreement with experimental data can be obtained (see Figure S12). As an example, for [Mn(II)(tpa)Cl_2] the error value decreases from 2.13 to 1.31 by using an S_0^2 value of 0.73. We note that reasonable estimates for the S_0^2 values are generally in the range of 0.85−1.0, however, further reduction in this value may also be attributed to errors in background subtraction. It may also be the case that the reduction in the S_0^2 values is somewhat artificial and is partially compensating for errors in the DW values. We note that for [Mn(II)(terpy)Cl_2] the $Calc_{DFT,DM-ref}$ fit together with a refined S_0^2 value has a χ^2 value which is identical to the fit data. While this appears to be a promising approach to reducing the number of free parameters, it unfortunately does not hold for the other two monomers. Modifying the S_0^2 value uniformly decreases the entire spectral intensity, hence, such an approach is not appropriate when the relative intensities of the contributions vary, as is the case with the dimeric complexes (*vide infra*). These results thus suggest that while part of the error derives from errors in amplitudes, a uniform scaling of the calculated spectra to the experiment is likely not sufficient to compensate for the discrepancies between theory and experiment. Nonetheless, for the monomeric complexes, the FEFF predications are able to capture the dominant spectral features.

Fits to the Mn Dimers EXAFS Data. Given the ability of FEFF to capture the dominant spectral features in the Mn monomers, it is of interest to extend these correlations to more complex Mn dimers. Figure 4 shows the fits to the Mn dimers, with the corresponding fit parameters summarized in Table 4, column 1. The fits show good agreement with the experimental EXAFS, with error values (reduced χ^2) ranging from 0.18 to 0.45 over the dimer series. Similar to the monomers, the fit distances are reasonably close to the crystallographic distances.

FEFF Calculated EXAFS Spectra for the Mn Dimers: $Calc_{XRD,CD}$, $Calc_{DFT,CD}$, and $Calc_{DFT,DM}$ Methods. The FEFF spectra calculated using the $Calc_{XRD,CD}$, $Calc_{DFT,CD}$, and $Calc_{DFT,DM}$ methods (first-principle calculations in the absence of fitting) are shown in Figure 5. In contrast to the monomers,

DOI: 10.1021/jacs.5b00783
J. Am. Chem. Soc. 2015, 137, 12815−12834

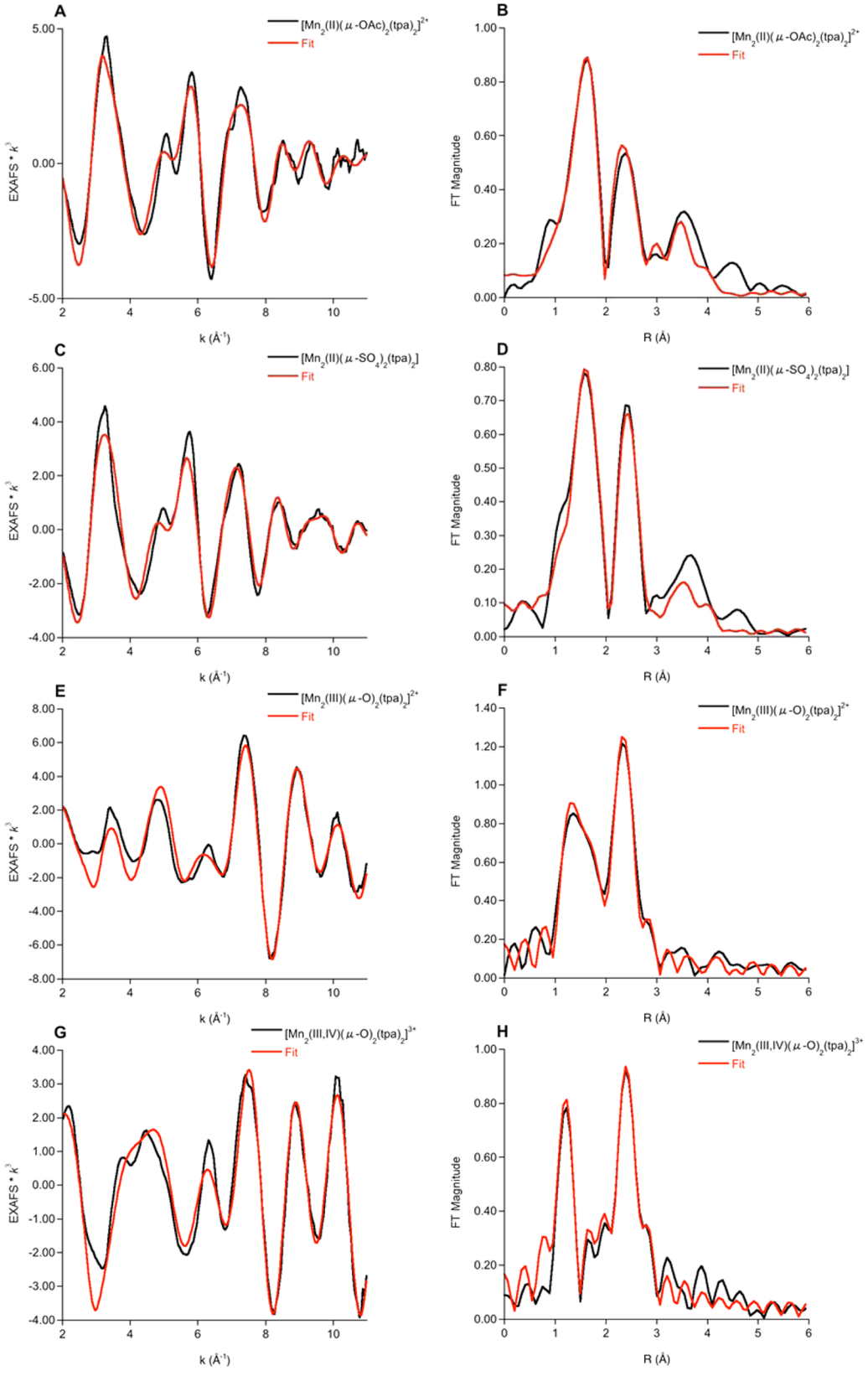

Figure 4. Experimental (black) and fits (red) to the $\chi(k)$ spectra and the corresponding non-phase shift corrected FTs of $[Mn_2(II)(\mu\text{-}OAc)_2(tpa)_2]^{2+}$ (A and B), $[Mn_2(II)(\mu\text{-}SO_4)_2(tpa)_2]$ (C and D), $[Mn_2(III)(\mu\text{-}O)_2(tpa)_2]^{2+}$ (E and F), and $[Mn_2(III,IV)(\mu\text{-}O)_2(tpa)_2]^{3+}$ (G and H).

the agreement between theory and experiment is in most cases worse. In all cases, the outer shell contributions to the FT are poorly predicted (Figure 5, right), and in some cases even the first shell FT deviates significantly from experiment (Figure 5F,H). We note that the predicted outer shell FT intensities are particularly poor for the $[Mn_2(II)(\mu\text{-}OAc)_2(tpa)_2]^{2+}$ and $[Mn_2(II)(\mu\text{-}SO_4)_2(tpa)_2]$ dimers, which may be attributed to the more complex OAc and SO_4 bridging motifs (Figure 5B,D).

DOI: 10.1021/jacs.5b00783
J. Am. Chem. Soc. 2015, 137, 12815−12834

This is also reflected in the error values of the calculated dimer spectra, which increase from the fit error values by up to a factor of ~30 (Table 4). In order to discern the origins of these differences, each computational approach is examined in detail below.

$Calc_{XRD,CD}$ Method. Table 4 shows the differences between the FEFF calculations using the crystal structure (column 2) and the fits to the EXAFS data (column 1). Not only have the error values increased significantly compared to those of the fits, but the error values have also increased substantially relative to what was obtained for the monomers using the same method (Table 2, column 2). The first shell distances (R between ~1 and 2 Å), and in some cases the second shell distances (R between ~2 and 3 Å),

Table 4. Comparison of Path Distances and DW Factors of the Mn Dimer Fits to Those Calculated from the Crystal Structures Using the CD method in FEFF 9.1 and from the Geometry Optimized Structures Using Both the CD method in FEFF 9.1 and the DM Method in FEFF 9.1 with and without Distance Refinement[a]

path		fit	$Calc_{XRD,CD}$	$Calc_{DFT,CD}$	$Calc_{DFT,DM}$	$Calc_{DFT,DM\text{-}ref}$
		$[Mn_2(II)(\mu\text{-}OAc)_2(tpa)_2]^{2+}$				
Mn−O[b]	R (Å)	2.12 (±0.0051), 3.54 (±0.0113)	2.12, 3.59	2.13, 3.49	2.13, 3.49	2.05, 3.32
	σ^2 (Å^2)	0.0044 (±0.0009), 0.0046 (±0.0016)	0.0049, 0.0043	0.0088, 0.0164	0.0093, 0.0194	0.0093, 0.0194
Mn−N	R (Å)	2.28 (±0.0042)	2.28	2.27	2.27	2.23
	σ^2 (Å^2)	0.0049 (±0.0007)	0.0083	0.0082	0.0076	0.0076
Mn−C	R (Å)	3.10 (±0.0052)	3.13	3.12	3.12	3.09
	σ^2 (Å^2)	0.0084 (±0.0006)	0.0071	0.0066	0.0059	0.0059
Mn−Mn	R (Å)	4.11 (±0.0077)	4.20	3.99	3.99	4.09
	σ^2 (Å^2)	0.0030 (±0.0010)	0.0013	0.0015	0.0036	0.0036
Mn−C−O	R (Å)	4.50 (±0.0152)	4.42	4.42	4.42	4.48
	σ^2 (Å^2)	0.0037 (±0.0021)	0.0042	0.0048	0.0045	0.0045
error (reduced χ^2)[c]		0.227	1.58	1.69	1.63	1.51
refined S_0^2		0.941	0.789	0.696	0.694	0.660
error (S_0^2 refined)		0.200	1.43	1.23	1.15	0.668
		$[Mn_2(II)(\mu\text{-}SO_4)_2(tpa)_2]$				
Mn−O[b]	R (Å)	2.15 (±0.0034), 3.58 (±0.0707)	2.10, 3.34	2.09, 3.49	2.09, 3.49	2.12, 4.06
	σ^2 (Å^2)	0.0016 (±0.0005), 0.0034 (±0.0033)	0.0040, 0.0033	0.0055, 0.0037	0.0054, 0.0074	0.0054, 0.0074
Mn−N	R (Å)	2.33 (±0.0033)	2.30	2.29	2.29	2.32
	σ^2 (Å^2)	0.0029 (±0.0004)	0.0054	0.0109	0.0102	0.0102
Mn−C	R (Å)	3.14 (±0.0089)	3.15	3.13	3.13	3.14
	σ^2 (Å^2)	0.0068 (±0.0010)	0.0075	0.0075	0.0066	0.0066
Mn−Mn	R (Å)	4.23 (±0.0136)	4.42	4.06	4.06	4.24
	σ^2 (Å^2)	0.0058 (±0.0015)	0.0013	0.0017	0.0035	0.0035
Mn−S−O	R (Å)	3.42 (±0.0518)	3.42	3.44	3.44	4.05
	σ^2 (Å^2)	0.0035 (±0.0113)	0.0030	0.0063	0.0062	0.0062
Mn−O−O	R (Å)	3.91 (±0.0317)	3.86	3.88	3.88	4.41
	σ^2 (Å^2)	0.0037 (±0.0070)	0.0114	0.0194	0.0191	0.0191
error (reduced χ^2)		0.183	1.65	2.04	2.03	0.490
refined S_0^2		0.975	0.653	0.626	0.621	0.830
error (S_0^2 refined)		0.168	0.951	1.27	1.21	0.344
		$[Mn_2(III)(\mu\text{-}O)_2(tpa)_2]^{2+}$				
Mn−O	R (Å)	1.83 (±0.0023)	1.83	1.84	1.84	1.73
	σ^2 (Å^2)	0.0022 (±0.0002)	0.0027	0.0021	0.0024	0.0024
Mn−N	R (Å)	2.23 (±0.0138)	2.24	2.21	2.21	2.08
	σ^2 (Å^2)	0.0280 (±0.0029)	0.0137	0.0138	0.0143	0.0143
Mn−C	R (Å)	2.98 (±0.0087)	3.03	2.99	2.99	2.82
	σ^2 (Å^2)	0.0121 (±0.0012)	0.0064	0.0059	0.0062	0.0062
Mn−Mn	R (Å)	2.63 (±0.0022)	2.64	2.66	2.66	2.53
	σ^2 (Å^2)	0.0014 (±0.0002)	0.0013	0.0011	0.0015	0.0015
Mn−C−N	R (Å)	5.10 (±0.0312)	4.49	4.42	4.42	4.40
	σ^2 (Å^2)	0.0122 (±0.0056)	0.0112	0.0110	0.0110	0.0110
error (reduced χ^2)		0.452	4.90	5.12	4.87	1.40
refined S_0^2		0.954	0.554	0.539	0.567	1.013
error (S_0^2 refined)		0.419	3.68	3.91	3.92	1.36
		$[Mn_2(III,IV)(\mu\text{-}O)_2(tpa)_2]^{3+}$				
Mn−O	R (Å)	1.80 (±0.0035)	1.81	1.83	1.83	1.78
	σ^2 (Å^2)	0.0049 (±0.0003)	0.0027	0.0036	0.0040	0.0040
Mn−N	R (Å)	2.02 (±0.0061)	2.10	2.10	2.10	2.06
	σ^2 (Å^2)	0.0128 (±0.0007)	0.0046	0.0141	0.0145	0.0145
Mn−C	R (Å)	2.91 (±0.0054)	2.93	2.92	2.92	2.91
	σ^2 (Å^2)	0.0095 (±0.0007)	0.0059	0.0064	0.0068	0.0068
Mn−Mn	R (Å)	2.63 (±0.0030)	2.63	2.66	2.66	2.63

DOI: 10.1021/jacs.5b00783
J. Am. Chem. Soc. 2015, 137, 12815−12834

Table 4. continued

path		fit	$Calc_{XRD,CD}$	$Calc_{DFT,CD}$	$Calc_{DFT,DM}$	$Calc_{DFT,DM\text{-}ref}$
		$[Mn_2(III,IV)(\mu\text{-}O)_2(tpa)_2]^{3+}$				
	σ^2 (Å^2)	0.0021 (±0.0002)	0.0013	0.0009	0.0015	0.0015
Mn−C−N	R (Å)	3.21 (±0.0204)	3.23	3.19	3.19	3.16
	σ^2 (Å^2)	0.0127 (±0.0046)	0.0065	0.0065	0.0065	0.0065
error (reduced χ^2)		0.221	3.38	6.74	6.17	0.876
refined S_0^2		0.943	0.485	0.223	0.234	0.726
error (S_0^2 refined)		0.200	1.85	2.89	2.91	0.464

[a]All distances and DW factors shown are the average values for each scattering path. Standard deviations for the fit values are given in parentheses. [b]Two paths of this type were included in the fit to the data. The corresponding distances and DW factors are separated by commas. [c]A measure of the error value between the experimental data and the EXAFS calculated via each method, where reduced $\chi^2 = F/(\text{no. of points} - \text{no. of variables})$ and $F = \Sigma_i [k_i^3/(\Sigma_j k_j^3 |\chi^{expt}(k_j)|)]^2[\chi^{expt}(k_i) - \chi^{calc}(k_i)]^2$. In the case of the fit the error is between the data and the final fit to the data.

are very similar to the EXAFS fit distances, but there are larger discrepancies in the outer shells, particularly for $[Mn_2(II)(\mu\text{-}OAc)_2(tpa)_2]^{2+}$ and $[Mn_2(II)(\mu\text{-}SO_4)_2(tpa)_2]$.

Table 5 shows the differences between the calculations using the $Calc_{XRD,CD}$ method and the fits to the data. Again, we note that the reported scaling for the DW value reflects additional amplitude errors. The scaling factor for the calculated and fit distances for the first shell Mn−O and Mn−N paths ranges from 0.96 to 1.02, while those of the longer distance Mn−C single scattering and the multiple scattering paths range from 0.98 to 1.00 and 1.00 to 1.14, respectively. The distance differences for the Mn−Mn path greatly depend on the bridging structure in the dimer. For both the $[Mn_2(III)(\mu\text{-}O)_2(tpa)_2]^{2+}$ and $[Mn_2(III,IV)(\mu\text{-}O)_2(tpa)_2]^{3+}$ dimers (fit distance = 2.63 Å), there is very good agreement between crystal structure and fit values, with scaling factors of 0.99−1.00. The agreement for the $[Mn_2(II)(\mu\text{-}OAc)_2(tpa)_2]^{2+}$ and $[Mn_2(II)(\mu\text{-}SO_4)_2(tpa)_2]$ dimers is somewhat worse (scaling factor = 0.98 and 0.96). This is most likely due to the longer Mn−Mn distances in these complexes, due to the OAc and SO_4 bridging ligands.

As observed for the monomers, the agreement between calculated and fit DW values also differs for the first shell paths and the outer shell paths. As shown in Table 5, using the $Calc_{XRD,CD}$ method the average calculated DW factors for the Mn dimers differ from the fit DW factors by scaling factors of 0.40−2.76 for the first shell paths and by scaling factors 1.06−4.50 for the Mn−Mn path. The scaling factors for the outer shell paths range from 0.11 to 1.95, however only the single scattering contributions to the outer shell are shown in Table 5. These results provide further evidence that at a fixed S_0^2 value, the largest error in the FEFF calculated spectra is associated with the calculation of the mean-square deviation in the bond lengths.

$Calc_{DFT,CD}$ Method. The results of the calculations using the $Calc_{DFT,CD}$ method for the Mn dimers are summarized in Figure 5 and Tables 3 and 4. As was observed for the monomers, the geometry optimized distances are quite similar to the crystallographic distances, with notable exceptions being the longer distance Mn−Mn paths in $[Mn_2(II)(\mu\text{-}OAc)_2(tpa)_2]^{2+}$ and $[Mn_2(II)(\mu\text{-}SO_4)_2(tpa)_2]$, which is attributed to the more flexible nature of the bridging ligands (as noted above). Overall the root-mean-square deviations, excluding hydrogen atoms, between the crystallographic coordinates and the geometry optimized structures range from 0.124 to 0.538 Å, indicating generally very good agreement. Also similar to the monomers, there is essentially no change in the calculated DW values between the $Calc_{XRD,CD}$ and $Calc_{DFT,CD}$ methods, as seen in Table 4.

There are, however, small changes in the first shell FT intensities between the $Calc_{XRD,CD}$ and $Calc_{DFT,CD}$ methods, despite the calculated DW factors being almost identical. These intensity changes arise from differences in the bond length distribution, as was also observed for the monomers. This is more clearly seen in the deconvolution of $[Mn_2(II)(\mu\text{-}SO_4)_2(tpa)_2]$ as shown in Figure 6, specifically in the Mn−N contribution. The variation in individual Mn−N distances [2.25, 2.26, 2.31, and 2.36 Å (crystal structure, ΔR = 0.11 Å) vs 2.19, 2.23, 2.35, and 2.39 Å (geometry optimized structure, ΔR = 0.20 Å)] results in a higher calculated total first shell FT intensity for the $Calc_{XRD,CD}$ method than for the $Calc_{DFT,CD}$ method. In the case of the outer shell Mn−Mn path in $[Mn_2(II)(\mu\text{-}SO_4)_2(tpa)_2]$, the 0.36 Å decrease in distance compared to the crystal structure results in poorer agreement between the calculated and fit spectra compared to the spectrum using the crystallographic distance, despite this path having the same calculated DW value for both the crystallographic and geometry optimized structures (Table 3 and Figure 6, right). This again emphasizes the importance of calculating both accurate distances and accurate DW factors if one wishes to make accurate spectral predictions.

It should be noted that in the deconvolution of $[Mn_2(III)(\mu\text{-}O)_2(tpa)_2]^{2+}$ (Figure 6, left) the intensities of all the individual path contributions are almost identical, yet the total FT intensities are different between the $Calc_{XRD,CD}$ and $Calc_{DFT,CD}$ methods. This discrepancy in the deconvolution is most likely due to differences in the interference between the calculated paths.

$Calc_{DFT,DM}$ Method. The results of the FEFF calculated spectra using the DMDW code are summarized in Figure 5 and Tables 3 and 4. In general, the DW factors calculated using the $Calc_{DFT,DM}$ method differ from the fit values by scaling factors of 0.29−1.95 for the first shell paths, by 0.24−1.96 for outer shell paths and by 0.83−1.68 for the Mn−Mn path. These scaling factors are similar to those for methods 2 and 3 (first shell 0.40−2.76, outer shell 0.11−1.95, Mn−Mn 1.06−4.50), indicating that the $Calc_{DFT,DM}$ method can provide slightly better calculated DW values than either the $Calc_{XRD,CD}$ method or the $Calc_{DFT,CD}$ method, though the deviations are still significant. Unlike with the monomers, the spectra calculated using the $Calc_{DFT,DM}$ method are almost identical to those calculated using the $Calc_{DFT,CD}$ method, particularly for R < 3 Å. A quantitative assessment shows that while the DW values for the individual paths vary between the $Calc_{DFT,CD}$ method and the $Calc_{DFT,DM}$ method, the average values are sufficiently similar to result in nearly identical calculated spectra at R < 3 Å.

There are, however, more noticeable differences in the calculated spectra using these two methods at R > 3 Å for the

DOI: 10.1021/jacs.5b00783
J. Am. Chem. Soc. 2015, 137, 12815−12834

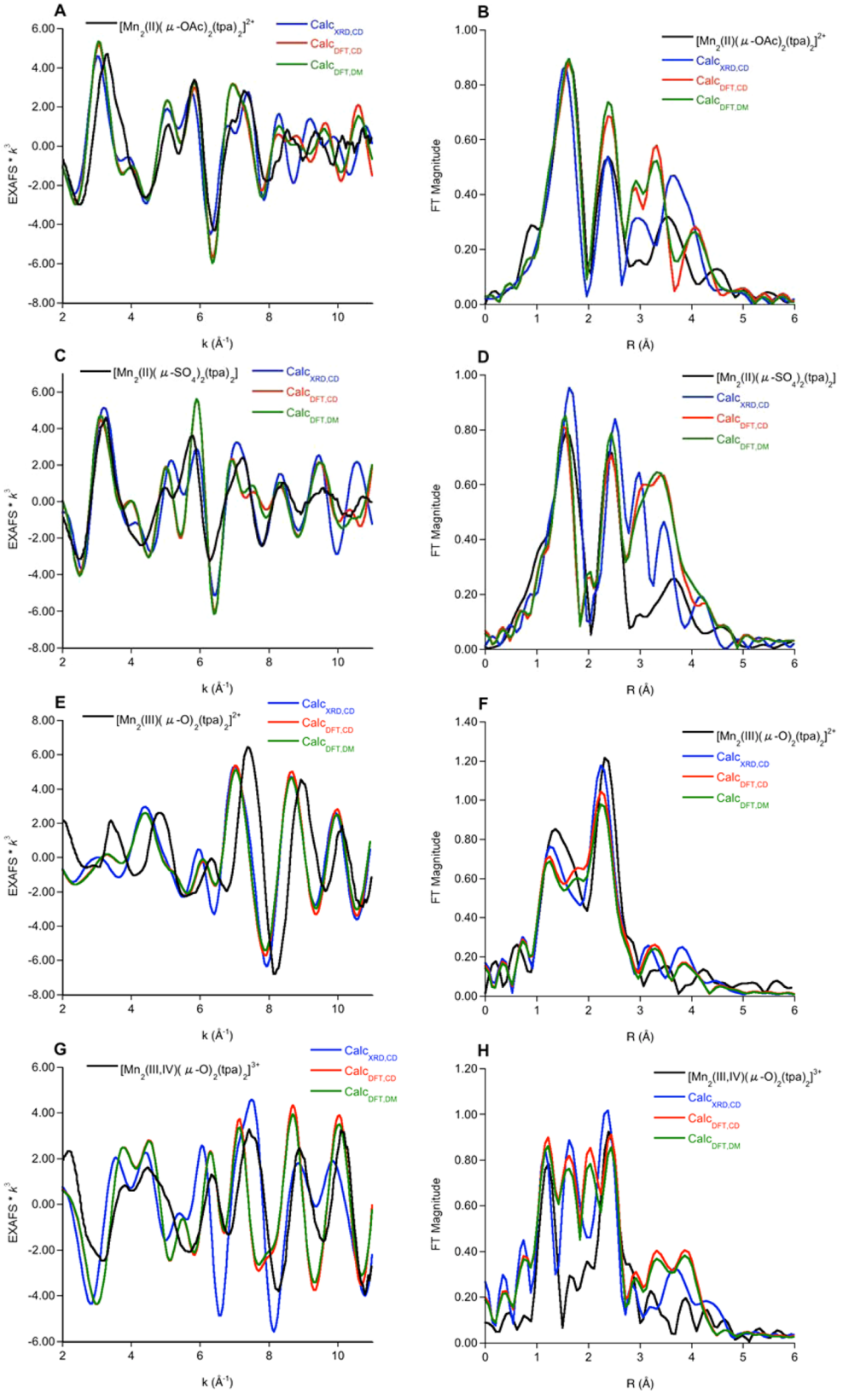

Figure 5. Experimental (black) and theoretical $\chi(k)$ spectra calculated using FEFF 9.1 and the corresponding non-phase shift corrected FTs of $[Mn_2(II)(\mu\text{-}OAc)_2(tpa)_2]^{2+}$ (A and B), $[Mn_2(II)(\mu\text{-}SO_4)_2(tpa)_2]$ (C and D), $[Mn_2(III)(\mu\text{-}O)_2(tpa)_2]^{2+}$ (E and F), and $[Mn_2(III,IV)(\mu\text{-}O)_2(tpa)_2]^{3+}$ (G and H). The calculations for the spectra using the $Calc_{DFT,CD}$ method included Debye temperatures determined using the sum of the first shell Mn−L stretching frequencies.

$[Mn_2(II)(\mu\text{-}OAc)_2(tpa)_2]^{2+}$ and $[Mn_2(II)(\mu\text{-}SO_4)_2(tpa)_2]$ dimers. As can be seen in the deconvolution of $[Mn_2(II)(\mu\text{-}SO_4)_2(tpa)_2]$ (Figure 6, right), these differences arise mainly from intensity differences in the Mn−Mn path, and to a lesser extent from

DOI: 10.1021/jacs.5b00783
J. Am. Chem. Soc. 2015, 137, 12815−12834

Table 5. Differences between the Final Fit Parameters and the FEFF 9.1 Calculated Parameters for the Mn Dimers, Using the $Calc_{XRD,CD}$, $Calc_{DFT,CD}$, $Calc_{DFT,DM}$, and $Calc_{DFT,DM\text{-}ref}$ Methods[a]

path		$Calc_{XRD,CD}$ (absolute deviation)	$Calc_{XRD,CD}$ (scaling factor)	$Calc_{DFT,CD}$ (absolute deviation)	$Calc_{DFT,CD}$ (scaling factor)	$Calc_{DFT,DM}$ (absolute deviation)	$Calc_{DFT,DM}$ (scaling factor)	$Calc_{DFT,DM\text{-}ref}$ (absolute deviation)	$Calc_{DFT,DM\text{-}ref}$ (scaling factor)
Mn−O 1.8−2.1 Å	ΔR (Å)	−0.04 to +0.01	1.00−1.02	−0.05 to +0.03	0.98−1.03	−0.05 to +0.03	0.98−1.03	−0.10 to −0.02	1.01−1.06
	$\Delta\sigma^2$ (Å^2)	−0.0022 to +0.0024	0.40−1.83	−0.0013 to +0.0044	0.29−1.37	−0.0009 to +0.0049	0.30−1.22	−0.0009 to +0.0049	0.30−1.22
Mn−N 2.0−2.3 Å	ΔR (Å)	−0.03 to +0.08	0.96−1.02	−0.04 to +0.08	0.96−1.02	−0.04 to +0.08	0.96−1.02	−0.15 to +0.04	0.98−1.07
	$\Delta\sigma^2$ (Å^2)	−0.0143 to +0.0034	0.54−2.76	−0.0142 to +0.0080	0.27−2.02	−0.0137 to +0.0073	0.29−1.95	−0.0137 to +0.0073	0.29−1.95
Mn−C 2.9−3.1 Å	ΔR (Å)	+0.01 to +0.05	0.98−1.00	−0.01 to +0.02	0.99−1.00	−0.01 to +0.02	0.99−1.00	−0.16 to 0	1.00−1.06
	$\Delta\sigma^2$ (Å^2)	−0.0057 to +0.0007	0.90−1.89	−0.0062 to +0.0007	0.90−2.04	−0.0059 to −0.0002	1.03−1.95	−0.0059 to −0.0002	1.03−1.95
Mn−Mn (short) 2.63 Å	ΔR (Å)	0 to +0.01	0.995−1.00	+0.03	0.99	+0.03	0.99	−0.08 to 0	1.00−1.04
	$\Delta\sigma^2$ (Å^2)	−0.0008 to −0.0001	1.06−1.59	−0.0012 to −0.0004	1.33−2.23	−0.0006 to +0.0001	0.95−1.43	−0.0006 to +0.0001	0.95−1.43
Mn−Mn (long) 4.1−4.2 Å	ΔR (Å)	+0.09 to +0.19	0.96−0.98	−0.17 to −0.12	1.03−1.04	−0.17 to −0.12	1.03−1.04	−0.02 to +0.01	1.00−1.01
	$\Delta\sigma^2$ (Å^2)	−0.0045 to −0.0017	2.31−4.50	−0.0041 to −0.0015	1.95−3.49	−0.0023 to +0.0006	0.83−1.68	−0.0023 to +0.0006	0.83−1.68

[a]Values have been obtained by subtracting the averaged fit values for a given path from the averaged calculated values for a given path. The scaling factor is the value by which the FEFF calculated parameter is multiplied in order to obtain the fit parameter (i.e., fit parameter = calculated parameter × scaling factor). We note that the deviation in the DW values also reflects other contributions to the amplitude errors (including S_0^2 and the background subtraction).

differences in the outer shell Mn−O path (average distance = 3.49 Å). The Mn−Mn DW values calculated using the $Calc_{DFT,DM}$ method are ca. two times larger than the DW values calculated using the $Calc_{DFT,CD}$ method (Table 4). In the case of $[Mn_2(II)(\mu\text{-}SO_4)_2(tpa)_2]$, the outer shell Mn−O DW also varies by a factor of 2 between the two methods. However, the total spectra are dominated by the changes in the Mn−Mn path. This highlights the fact that EXAFS is ideally suited for obtaining accurate Mn−Mn vectors, but more limited in defining the metrics of bridging light atoms.

FEFF Calculated EXAFS Spectra with Fit Distances for the Mn Dimers: The $Calc_{DFT,DM\text{-}ref}$ Method. As was done for the monomers, we also did a final set of fits for the dimers, in which the $Calc_{DFT,DM}$ calculated DW values were held fixed and the distances for each path were allowed to refine. As expected, the error values generally decrease relative to the $Calc_{DFT,DM}$ method. We also note that in some cases, fixing the DW values results in the distances refining to unreasonably short or long values, relative to the crystallographically determined distances. This is particularly pronounced for the outer shell contributions and likely results from fixing the DW at values that are far from a true minimum.

The Impact of S_0^2 Values on the Predicted Mn Dimer Spectra. As was also observed for the monomers, the agreement between the calculated spectra and experiment can be improved by refining the amplitude parameter, S_0^2 (Table 4). However, for the dimer fits, the refined S_0^2 values become in some cases unreasonably low (<0.5, Table 4). The fits with refined S_0^2 values can be found in Figure S13 (for the $Calc_{XRD,CD}$, $Calc_{DFT,CD}$, and $Calc_{DFT,DM}$ methods) and Figure S15 (for the $Calc_{DFT,DM\text{-}ref}$ method). While the error values uniformly decrease upon refining S_0^2, it is clear that major discrepancies remain in the FT intensity distribution. This indicates, as discussed above, that a significant portion of the error must be attributed to differential errors in the calculated DW values that may be either over or underestimated, depending on the specific scattering pathway and the nature and number of the scatterers involved.

Extension to Systems of Unknown Structure. The above analysis highlights the complexity of *a priori* calculations of EXAFS spectra for complexes of known structure. The challenges, of course, are even greater when one wants to apply this approach to understand unknown structures. However, the above analysis provides useful lessons, which can be used to constructively evaluate possible models. First, the analysis of the monomeric and dimeric complexes highlights the well-known strength of EXAFS in distance determination, particularly for first shell distances and heavy backscatterers at short distances (such as the ∼2.6 Å Mn−Mn distances in the dimers). We note, however, that as the Mn−Mn distances become longer, the $1/R^2$ distance dependence of EXAFS together with the increase in multiple scattering contributions from the ligand framework at longer distances increase the error in distance determination. This has also been a challenge in the reliable determination of the long ∼3.3 Å Mn−Mn distances in the OEC, where the overlap with the Mn−Ca vectors increases the uncertainty in the distance determinations. The ability to use the EXAFS to reliably predict the presence of long Mn−Mn distances has also been noted by Li et al.[17] While the ability to obtain range-extended EXAFS can certainly improve the ability to determine long Mn−Mn vectors, such experiments are still far from routine.[13] Further, we note that for FT peaks of low amplitude, Fourier truncation effects can further contribute to the errors.

The present study also demonstrates that significant errors in the prediction of EXAFS spectra are associated with the reliable determination of amplitudes. The errors in amplitudes may have contributions from errors in the DW values, the S_0^2 parameters, and the background subtraction. We note, however, that in the case of the dimeric complexes the relative amplitudes were shown to be incorrect, indicating that a simple linear scaling of the amplitude is not sufficient. One must account for possible

DOI: 10.1021/jacs.5b00783
J. Am. Chem. Soc. 2015, 137, 12815−12834

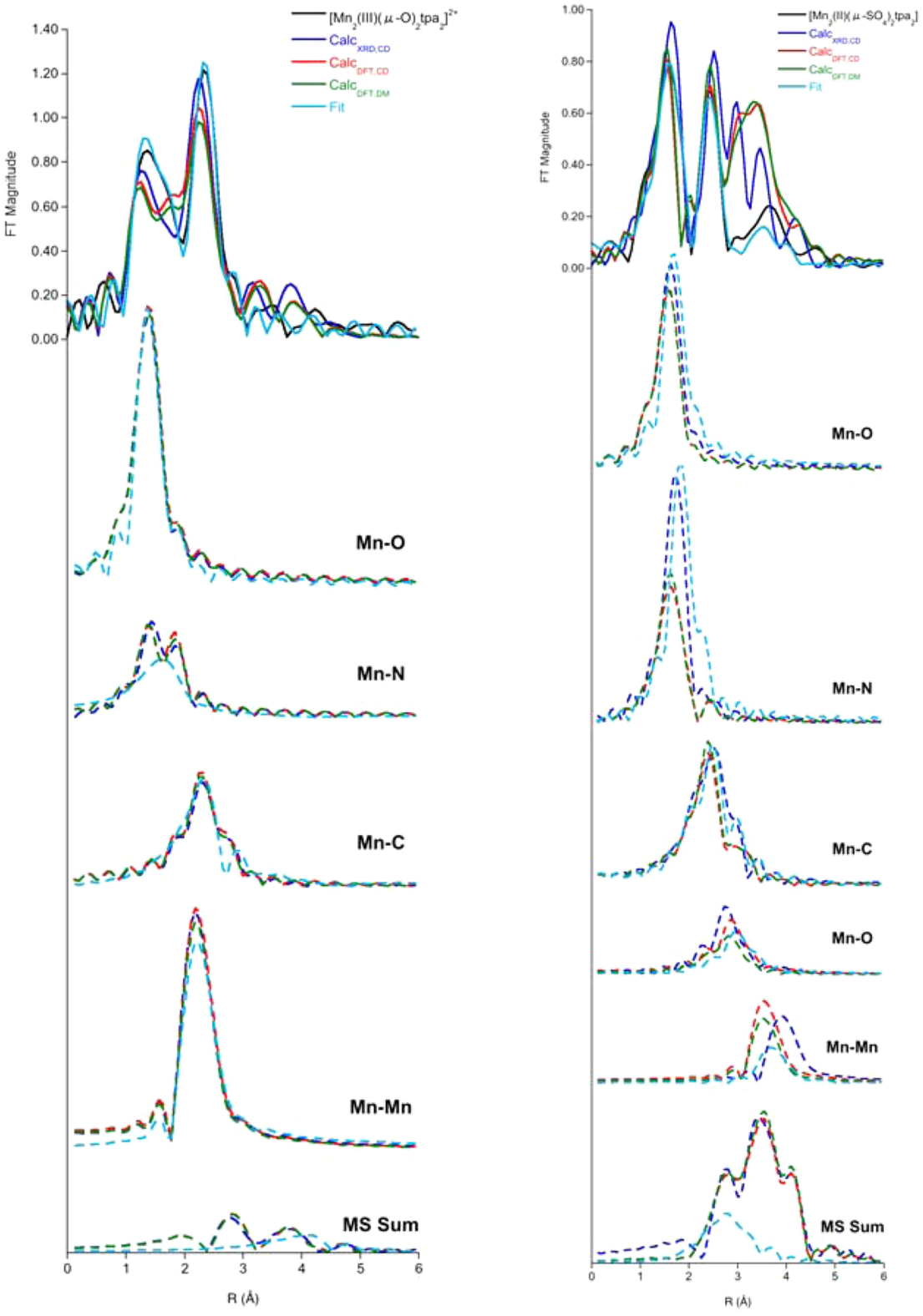

Figure 6. Calculated spectra and significant single and multiple scattering contributions for $[Mn_2(III)(\mu\text{-}O)_2(tpa)_2]^{2+}$ (left) and $[Mn_2(II)(\mu\text{-}SO_4)_2(tpa)_2]$ (right). The path deconvolutions for each method are the sums of the individual scattering paths of each type. The calculations for the spectra using the $Calc_{DFT,CD}$ method included Debye temperatures determined using the sum of the first shell Mn−L stretching frequencies. Spectra have been offset on the *y*-axis, but share a common *y*-scale.

differential error in the DW values, which thus result in relative modulation of the FT peaks. On a more positive note, the present results demonstrate that one can in general reliably determine FT peak positions. By using the lessons determined for the crystallographically characterized monomers and dimers, a range of calculated amplitudes that could be consistent with the experimentally observed amplitudes may be established. We note, as discussed above, that the exact origin of the amplitude

DOI: 10.1021/jacs.5b00783
J. Am. Chem. Soc. 2015, 137, 12815−12834

error is complicated by correlation of S_0^2 with the DW values and the added uncertainty resulting from experimental extraction of the EXAFS signal. Hence in the section which follows, we restrict the discussion to calculated spectra with fixed S_0^2 values and use the error analysis detailed above (Tables 3 and 5) to establish reasonable ranges for DW values, thus limiting the possible phase space. Further, we compare only to published background subtracted data, recognizing that this may result in additional amplitude errors.

Application to the OEC. Herein, the above-described analysis is extended to the S_1 state EXAFS data of the OEC in PSII. The goal is to evaluate the range of possible models that could be consistent with the known data, given our understanding of errors in the amplitudes. As discussed above, additional errors may arise from the chosen structural model. Here, we limit the investigation to the six literature models shown in Scheme 2. Models **A**,[24] **B**,[25] and **C**[26] share the same spatial arrangement of Mn, Ca and O atoms of the core, but differ in the exact connectivity and the interatomic distances (see Table 1). Model **D**[27,61] features a Mn_3O_4Ca cubane with a Cl^- ion bound to Ca and the fourth Mn ion connected to one μ_3-oxo-bridge. Models **E** and **F**[14,28] have approximately the same Mn-oxo core connectivity: Mn1, Mn2, and Mn3 share μ_2- and μ_3-oxo bridges, and Mn4 is attached to Mn3 with two μ_2-oxo bridges. Models **E** and **F**[28] differ in the position of the Ca ion, which is linked to the μ_3-oxo bridge in model **E**, but connected to the μ_2-oxo bridges in model **F**.

Figure 7 (top) compares the predicted FT spectra for the OEC of a PSII monomer in the recently reported XFEL structure from Suga et al. (model **A**)[24] and the previously reported synchrotron radiation (SR) XRD structure from Umena et al. (model **B**).[25] Model **B** clearly shows poor R-space agreement with the experimental FT (with a χ^2 value of 8.5 relative to experiment), consistent with the fact that the SR XRD structure is generally agreed to have undergone beam-induced reduction, resulting in longer Mn−O and Mn−Mn bond lengths (Table 1).[11,18,63,66,67] Model **A** in contrast shows far better agreement with experiment in the outer shell Mn−Mn peak, with the χ^2 value decreasing to 5.0. This is consistent with the fact that the EXAFS and XFEL XRD derived Mn−Mn distances are nearly identical. Interestingly, however, the Mn−O peak (though at a shorter distance than model **A**) is still too long (by ∼0.1 Å) relative to the experimental S_1 EXAFS data. We note that while the present model study has indicated that significant errors exist in the prediction of EXAFS amplitude, the first shell and metal−metal distances should be accurate within a few tenths of an Ångstrom There are several possible factors that could contribute to the discrepancy between the EXAFS predicted data based on the XFEL structure and the experimental EXAFS data. The differences may reflect errors in the ability to accurately determine the Mn−O distance at 1.95 Å resolution[20,68,69] and/or the presence of photoreduced Mn.[68,69] We note that the long 2.38 Å Mn4−O5 vector in the XFEL structure has been suggested to indicate protonation of O5.[70] However, in the context of the present study, O5 is found to make no significant contribution to the calculated FT spectrum (see Figure S16), indicating that the origin of the discrepancies between the experimental EXAFS spectrum and theory lie elsewhere. Further, we note that a recent study by Pushkar et al. has demonstrated smaller discrepancies between the XFEL structure and the RT EXAFS.[20] However, in their study global DWs were utilized, and any additional parameters that were refined in their EXAFS simulations are unfortunately not specified, making a one-to-one comparison with the present

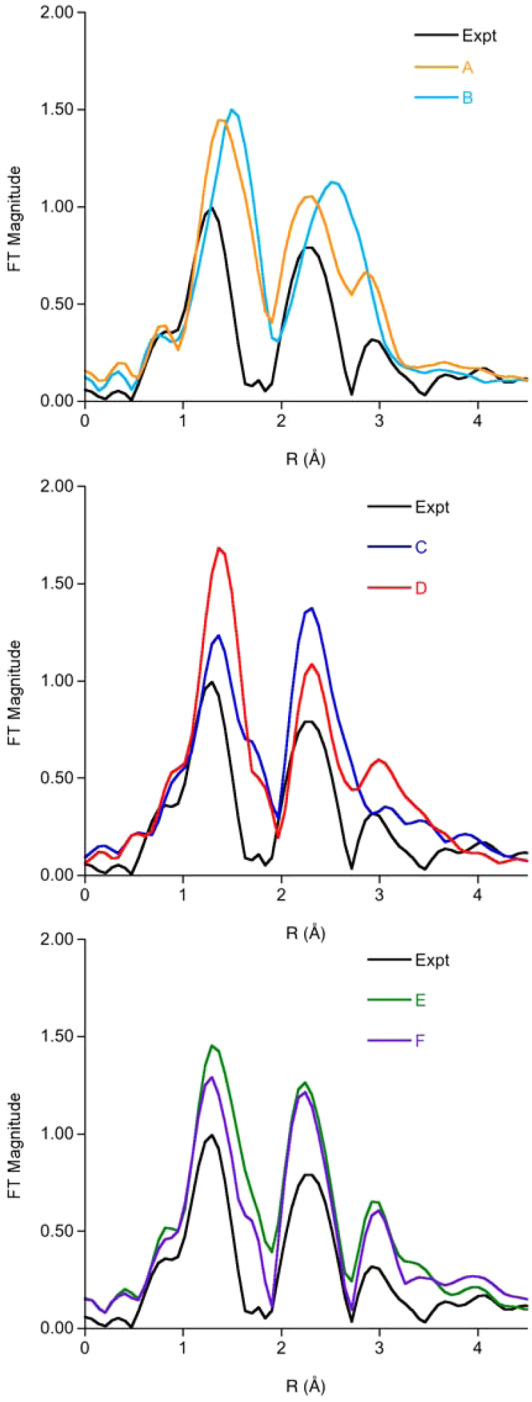

Figure 7. FT of the experimental EXAFS spectrum of the OEC S_1 state (black),[18] and the calculated FTs of the EXAFS of the OEC active site using the recent Suga et al. XFEL crystal structure (**A**) and the previous Umena crystal structure (**B**) (top), the Siegbahn (**C**), and Batista (**D**) models (center) and the Pantazis et al. models based on polarized EXAFS cores (**E**, **F**) (bottom). All spectra of the models were calculated using FEFF 9.1 and the correlated Debye model using a Debye temperature of 1000 K.

study prohibitive. We do note, however, that Pushkar et al. do see small differences in the distances, which they largely attribute to errors in crystallographic bond distance determinations, as noted above. They also argue that the interconversion between closed and open cubane conformations (which is relevant for the S2 state)[67] would be observable in the FT amplitudes. However, in

DOI: 10.1021/jacs.5b00783
J. Am. Chem. Soc. 2015, 137, 12815−12834

light of the present study and the errors we have demonstrated in accurately determining amplitudes, we do not concur with this assessment.

Finally, in the present context, we note that the possibility of XFEL-induced damage to crystal structures remains a controversial, albeit very important topic. A recent study by Hau-Reige and Bennion showed that even on the femtosecond time scales used for XFEL XRD damage can be observed.[71] In their study of the iron sulfur protein ferredoxin, it was shown that atomic displacements occur in the vicinity of the metal active site, with the largest atomic displacements occurring for lighter atoms. This would be consistent with accurate Mn−Mn vectors but expanded Mn−O vectors in the XFEL XRD. We note that Suga et al. did use a lower dose than Hau-Reige and Bennion, however, recent studies caution against the generalizability of simple dose damage correlations.[72] Hence, the origin of the differences between the S_1 state EXAFS data and the XFEL XRD remains an open question. We note, however, in the context of the present study, observable differences in the predicted EXAFS for the XFEL structure and the experimental EXAFS spectrum are observed. In our view, these results highlight the continued important role that EXAFS will play in the validation of distances.

The ability to relate the EXAFS data to a unique topological conformation in the OEC also must be addressed. For this reason, we have calculated the EXAFS for four different computationally based models shown in Scheme 2. Model **C** corresponds to the S_1-state model proposed by Siegbahn, while model **D** is Siegbahn's cluster model adaptation of an older QM/MM model by Batista. Models **E** and **F** represent topologically different cores, which were inferred from polarized EXAFS studies. Detailed metrics of each core can be found in the Experimental Section and in the SI. Inspection of Figure 7 clearly shows that all four of these models have average Mn−O and Mn−Mn vectors that are in agreement with experiment. However, due to the inability to accurately predict the amplitudes, as highlighted for the monomer and dimer cases in the first section of this paper, any of these four topologically varied models could correspond to the experimental EXAFS data. Similarly we note that Dau and co-workers have argued for different S_1-state metrics based on their EXAFS analyses.[12] However, in light of the present results it appears that much of the differences between the Yano et al.[10,14,15] and Dau et al.[11,12] results may derive from limitations in amplitude predictions/modeling, which will also affect coordination numbers. We note, however, that the Mn−Mn coordination numbers and distances reported by Yano et al. matches with the numbers obtained from the XFEL crystallography data.[10,14,24] While numerous independent studies[24,69] now indicate that model **C** represents the correct topology for the S_1 state, the present study highlights the fact that the ability to distinguish different topologies by EXAFS is intrinsically limited. In fact of models **C**−**F**, **C** has the highest χ^2 value of 4.4, while the values decrease to 4.2, 2.9, and 2.1 for models **D**, **E**, and **F**, respectively. We emphasize, however, that any of these four models could be consistent with the EXAFS data in the absence of other experimental constraints. Our results are also consistent with the observations of Li et al., who showed that the ability to use EXAFS data to uniquely determine the presence or absence of longer Mn−Mn vectors in the OEC active site is limited.[17]

To illustrate the uncertainty in calculated amplitudes, Figure 8 shows the FT of the experimental S_1-state data along with the spectra of model **C** calculated using the upper and lower limits of the DW values based on the scale factor ranges obtained from the Mn dimer model complexes (Table 5). The spectra calculated using the upper limit DW values in Table 5 generally have FT intensities that are still too high relative to experiment. As such, Figure 8 also shows the FTs of the spectra calculated with DW values "damped" to the degree that theory and experiment reasonably agree. For model **C**, the DW values must be "damped" by factors of 1.8 and 5.3 for the Mn−O and Mn−Mn contributions, respectively. The asymmetry in the scaling factors highlights that the amplitude errors cannot be simply attributed to the S_0^2 values. These are both larger than the corresponding scale factors of 1.37 (Mn−O) and 2.23 (Mn−Mn) in Table 5. The "damped" DW scale factor for the Mn−C contribution does not change from that in Table 5. The necessity to further damp the DW values relative to the estimates derived from our model studies suggests that in the protein data, even greater disorder is present. This may manifest itself not only as static disorder, as discussed above, but also conformational disorder.[15]

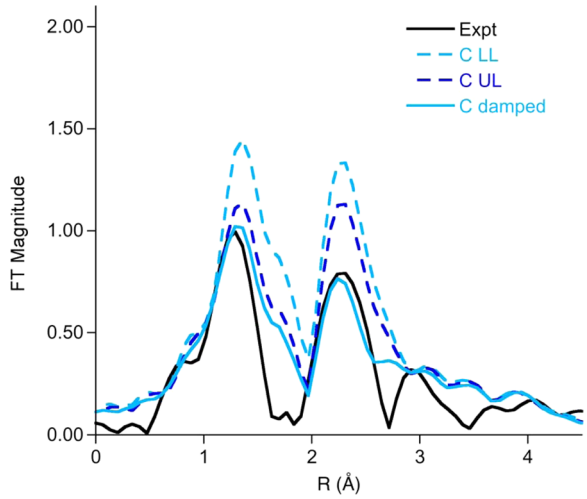

Figure 8. FT of the experimental EXAFS spectrum of the PS II S_1 state (solid black)[18] and the calculated FTs of the EXAFS of model **C** using the lower (dashed light blue) and upper (dashed dark blue) limits of the DW values based on those from the Mn dimer model complexes. The calculated FT using "damped" upper limit DW values needed to match the experimental FT is also shown (solid light blue).

We note that the "damped" spectra in Figure 8 also better highlight the differences between the experimental and calculated spectra. While the short Mn−O and Mn−Mn vectors are clearly well predicted, there are differences in the ∼2 Å range of the FT (corresponding to ∼2.3 Å upon phase shift correction). It appears that all of the calculated models have too much intensity in this range. This likely corresponds to the long Mn−O(H_2O) vectors for which the calculated DW is likely too low. Disorder in the Mn−O(H_2O) vectors in the experimental data may explain the absence of this feature.

In summary, the analysis of the predicted FTs for various OEC models emphasizes the robustness of EXAFS for distance determination, but highlights the limitations of EXAFS in terms of amplitudes and hence also three-dimensional topological information. This has important implications for future comparisons of experimental and calculated EXAFS data of other S states of PSII as well as other active sites in biological systems.

CONCLUSIONS AND DISCUSSION

A systematic study of the fit and predicted EXAFS spectrum of a series of Mn monomers and dimers has been presented in order to assess the accuracy of spectra calculated from known

DOI: 10.1021/jacs.5b00783
J. Am. Chem. Soc. 2015, 137, 12815−12834

crystallographic models and by extension the accuracy of the calculated EXAFS when applied to more complex systems, such as the OEC of PSII.

As expected, the values obtained from least-squares fitting of the FEFF calculated parameters to the experimental EXAFS spectra produced good fits, which were generally in good agreement with the small molecule crystallographic data. However, limitations do exist, particularly with regard to the prediction of longer distances. This is consistent with the $1/R^2$ dependence of the EXAFS signal and has been amply noted in the literature.

The more intriguing question that has motivated this study—how accurately can one predict EXAFS spectra from first-principles without any fitting or recourse to experimental data—has, however, a different answer. The present study demonstrates that while distances are generally accurately predicted from EXAFS calculations (particularly for first shell distances or strong backscatterers), significant errors exist in the calculated amplitudes that thus greatly limit the predictive ability of this approach. A considerable component of the uncertainty is the difficulty of predicting accurate amplitudes in EXAFS, including DW factors, S_0^2, and scattering amplitudes. Thus, while one can generally validate the position of a peak in the FT through theory, neither the absolute nor relative amplitude of FT peaks can be accurately predicted. For all complexes, the DW factors calculated using the correlated Debye model at either optimized or experimental structures were nearly identical. Using the much more sophisticated DM method ($Calc_{DFT,DM}$) can in most cases slightly improve the agreement between calculated and fit values but, unfortunately, not to the extent that accurate predictions of EXAFS spectra are obtained. Structural uncertainties introduce further complications in the ability to accurately predict EXAFS spectra. The shortcomings of the theoretically predicted EXAFS spectra were particularly pronounced for the dimers included in this work: how well the calculated distances and amplitudes were predicted depended on the bridging structure in the dimer. Both distances and DW factors were closer to those in the experiment for the shorter Mn−Mn distances resulting from the $(\mu\text{-O})_2$ bridging motif. Nevertheless, the amplitude errors are not strongly correlated with phase errors, which are important for distance determinations.

We emphasize this point so strongly because there have been multiple attempts in the literature to back up experimentally obtained EXAFS spectra by recourse to theoretically calculated ones, in particular with respect to the oxygen-evolving complex in photosystem II.[14,19,20] We show here the use of such predicted spectra must be approached with extreme caution, particularly with regard to the amplitudes and the outer shell contributions. Hence, while both crystallographic models **A** and **B** show deviations with regard to the experimental data, any of the computational models **C**−**F** agrees reasonably with experiment despite the large topological variations. Hence, based on EXAFS data, no sound conclusions that favor one structure over the other can be drawn. Previous attempts that claimed the contrary were all based on EXAFS modeling that was at most as sophisticated as our $Calc_{DFT,CD}$ method, but mostly invoked the even less accurate approach of using global DW factors.[14,18−20] The results herein show that the predictability of EXAFS spectra using current state of the art methods may not be sufficiently discriminative to distinguish the debated structural motifs. To achieve this goal, it is therefore necessary to combine this approach with state-specific information on other properties of the system, such as those obtained from EPR/ENDOR and Mn K-pre-edge XAS spectroscopies.[69,73]

We believe that the conclusions of this work have far reaching implications for the use of theoretical EXAFS modeling, not only in biochemistry but in all major branches of chemistry where EXAFS analysis plays an important role. We take this work as motivation and inspiration to direct future efforts toward improving the theoretical prediction of EXAFS spectra to make it an even more powerful partner of experimental investigations.

■ ASSOCIATED CONTENT

Supporting Information

The Supporting Information is available free of charge on the ACS Publications website at DOI: 10.1021/jacs.5b00783.

Additional details for EXAFS fitting procedures and computational protocols (PDF)

Crystallographic data for [Mn2(II)(μ-SO4)2(tpa)2]·3H_2O·2CH_3OH (CIF)

■ AUTHOR INFORMATION

Corresponding Authors

*jjr@uw.edu

*frank.neese@cec.mpg.de

*serena.debeer@cec.mpg.de

Present Addresses

[∇]Physical and Life Sciences Directorate, Lawrence Livermore National Laboratory, Livermore, California 94550, United States

[○]von Liebig Science Center, Juanita College, Huntingdon, Pennsylvania 16652, United States

Notes

The authors declare no competing financial interest.

■ ACKNOWLEDGMENTS

S.D. and F.N. thank the Max Planck Society for funding. S.D. acknowledges Cornell University and the Alfred P. Sloan Foundation. J.P., M.G., C.D., and M.-N.C. are grateful to the French National Agency (ANR) (grant nos. ANR-13-BS07-0015-01; MnCaOEC; and ANR-09-JCJC-0087; MANGACOM) and the LABEX program ARCANE (grant no. ANR-11-LABX-0003-01) for financial support. Portions of these data were carried out at the Stanford Synchrotron Radiation Lightsource (SSRL), a national user facility operated by Stanford University on behalf of the U.S. Department of Energy, Office of Basic Energy Sciences. J.Y. thanks the Director of the Office of Science, Office of Basic Energy Sciences (OBES), Division of Chemical Sciences, Geosciences, and Biosciences, DOE, under contract DE-AC02-05CH11231.

■ REFERENCES

(1) Cramer, S. P.; Hodgson, K. O.; Gillum, W. O.; Mortenson, L. E. *J. Am. Chem. Soc.* **1978**, *100*, 3398.

(2) Kirby, J. A.; Robertson, A. S.; Smith, J. P.; Thompson, A. C.; Cooper, S. R.; Klein, M. P. *J. Am. Chem. Soc.* **1981**, *103*, 5529.

(3) Shu, L. J.; Nesheim, J. C.; Kauffmann, K.; Munck, E.; Lipscomb, J. D.; Que, L. *Science* **1997**, *275*, 515.

(4) Riggs-Gelasco, P. J.; Shu, L. J.; Chen, S. X.; Burdi, D.; Huynh, B. H.; Que, L.; Stubbe, J. *J. Am. Chem. Soc.* **1998**, *120*, 849.

(5) Stone, K. L.; Behan, R. K.; Green, M. T. *Proc. Natl. Acad. Sci. U. S. A.* **2005**, *102*, 16563.

(6) Behan, R. K.; Green, M. T. *J. Inorg. Biochem.* **2006**, *100*, 448.

(7) Lee, S. K.; DeBeer George, S.; Antholine, W. E.; Hedman, B.; Hodgson, K. O.; Solomon, E. I. *J. Am. Chem. Soc.* **2002**, *124*, 6180.

(8) Dau, H.; Grundmeier, A.; Loja, P.; Haumann, M. *Philos. Trans. R. Soc., B* **2008**, *363*, 1237.

(9) Dau, H.; Liebisch, P.; Haumann, M. *Phys. Scr.* **2005**, *T115*, 844.

DOI: 10.1021/jacs.5b00783
J. Am. Chem. Soc. 2015, 137, 12815−12834

(10) Glöckner, C.; Kern, J.; Broser, M.; Zouni, A.; Yachandra, V.; Yano, J. *J. Biol. Chem.* **2013**, *288*, 22607.
(11) Grundmeier, A.; Dau, H. *Biochim. Biophys. Acta, Bioenerg.* **2012**, *1817*, 88.
(12) Haumann, M.; Muller, C.; Liebisch, P.; Iuzzolino, L.; Dittmer, J.; Grabolle, M.; Neisius, T.; Meyer-Klaucke, W.; Dau, H. *Biochemistry* **2005**, *44*, 1894.
(13) Pushkar, Y.; Yano, J.; Glatzel, P.; Messinger, J.; Lewis, A.; Sauer, K.; Bergmann, U.; Yachandra, V. *J. Biol. Chem.* **2007**, *282*, 7198.
(14) Yano, J.; Kern, J.; Sauer, K.; Latimer, M. J.; Pushkar, Y.; Biesiadka, J.; Loll, B.; Saenger, W.; Messinger, J.; Zouni, A.; Yachandra, V. K. *Science* **2006**, *314*, 821.
(15) Yano, J.; Yachandra, V. *Chem. Rev.* **2014**, *114*, 4175.
(16) Li, X. C.; Siegbahn, P. E. M.; Ryde, U. *Proc. Natl. Acad. Sci. U. S. A.* **2015**, *112*, 3979.
(17) Li, X.; Sproviero, E. M.; Ryde, U.; Batista, V. S.; Chen, G. *Int. J. Quantum Chem.* **2013**, *113*, 474.
(18) Luber, S.; Rivalta, I.; Umena, Y.; Kawakami, K.; Shen, J. R.; Kamiya, N.; Brudvig, G. W.; Batista, V. S. *Biochemistry* **2011**, *50*, 6308.
(19) Sproviero, E. M.; Gascon, J. A.; McEvoy, J. P.; Brudvig, G. W.; Batista, V. S. *J. Am. Chem. Soc.* **2008**, *130*, 6728.
(20) Pushkar, Y. N.; Davis, K. M. *J. Phys. Chem. B* **2015**, *119*, 3492.
(21) Hsiao, Y. W.; Tao, Y.; Shokes, J. E.; Scott, R. A.; Ryde, U. *Phys. Rev. B* 2006, *74*, 214101.
(22) Ryde, U. *Dalton Trans.* **2007**, 607.
(23) Rehr, J. J.; Kas, J. J.; Prange, M. P.; Sorini, A. P.; Takimoto, Y.; Vila, F. *C. R. Phys.* **2009**, *10*, 548.
(24) Suga, M.; Akita, F.; Hirata, K.; Ueno, G.; Murakami, H.; Nakajima, Y.; Shimizu, T.; Yamashita, K.; Yamamoto, M.; Ago, H.; Shen, J. R. *Nature* **2015**, *517*, 99.
(25) Umena, Y.; Kawakami, K.; Shen, J. R.; Kamiya, N. *Nature* **2011**, *473*, 55.
(26) Siegbahn, P. E. M. *Biochim. Biophys. Acta, Bioenerg.* **2013**, *1827*, 1003.
(27) Sproviero, E. M.; Gascon, J. A.; McEvoy, J. P.; Brudvig, G. W.; Batista, V. S. *J. Am. Chem. Soc.* **2008**, *130*, 3428.
(28) Pantazis, D. A.; Orio, M.; Petrenko, T.; Zein, S.; Lubitz, W.; Messinger, J.; Neese, F. *Phys. Chem. Chem. Phys.* **2009**, *11*, 6788.
(29) Shoji, M.; Isobe, H.; Yamanaka, S.; Umena, Y.; Kawakami, K.; Kamiya, N.; Shen, J. R.; Nakajima, Y.; Yamaguchi, K. *Mol. Phys.* **2015**, *113*, 359.
(30) Shoji, M.; Isobe, H.; Yamanaka, S.; Umena, Y.; Kawakami, K.; Kamiya, N.; Shen, J. R.; Nakajima, Y.; Yamaguchi, K. *Adv. Quantum Chem.* **2015**, *70*, 325.
(31) Duboc, C.; Phoeung, T.; Zein, S.; Pécaut, J.; Collomb, M. N.; Neese, F. *Inorg. Chem.* **2007**, *46*, 4905.
(32) Mantel, C.; Baffert, C.; Romero, I.; Deronzier, A.; Pécaut, J.; Collomb, M. N.; Duboc, C. *Inorg. Chem.* **2004**, *43*, 6455.
(33) Mantel, C.; Chen, H. Y.; Crabtree, R. H.; Brudvig, G. W.; Pécaut, J.; Collomb, M. N.; Duboc, C. *ChemPhysChem* **2005**, *6*, 541.
(34) Collomb, M.-N.; Mantel, C.; Romain, S.; Duboc, C.; Leprêtre, J.-C.; Pécaut, J.; Deronzier, A. *Eur. J. Inorg. Chem.* **2007**, *2007*, 3179.
(35) Towle, D. K.; Botsford, C. A.; Hodgson, D. J. *Inorg. Chim. Acta* **1988**, *141*, 167.
(36) Romain, S.; Baffert, C.; Duboc, C.; Lepretre, J. C.; Deronzier, A.; Collomb, M. N. *Inorg. Chem.* **2009**, *48*, 3125.
(37) Romain, S.; Duboc, C.; Neese, F.; Riviere, E.; Hanton, L. R.; Blackman, A. G.; Philouze, C.; Lepretre, J. C.; Deronzier, A.; Collomb, M. N. *Chem. - Eur. J.* **2009**, *15*, 980.
(38) Strautmann, J. B. H.; DeBeer George, S.; Bothe, E.; Bill, E.; Weyhermueller, T.; Stammler, A.; Boegge, H.; Glaser, T. *Inorg. Chem.* **2008**, *47*, 6804.
(39) Tenderholt, A.; Hedman, B.; Hodgson, K. O. In *X-Ray Absorption Fine Structure, XAFS13*; Hedman, B., Painetta, P., Eds.; AIP Publishing LLC: Melville, NY, 2007; Vol. *882*, p 105.
(40) Ankudinov, A. L.; Rehr, J. J. *Phys. Rev. B: Condens. Matter Mater. Phys.* **1997**, *56*, R1712.
(41) Rehr, J. J.; Kas, J. J.; Vila, F. D.; Prange, M. P.; Jorissen, K. *Phys. Chem. Chem. Phys.* **2010**, *12*, 5503.
(42) Oshio, H.; Ino, E.; Mogi, I.; Ito, T. *Inorg. Chem.* **1993**, *32*, 5697.
(43) Hitomi, Y.; Ando, A.; Matsui, H.; Ito, T.; Tanaka, T.; Ogo, S.; Funabiki, T. *Inorg. Chem.* **2005**, *44*, 3473.
(44) Dubois, L.; Pécaut, J.; Charlot, M.-F.; Baffert, C.; Collomb, M.-N.; Deronzier, A.; Latour, J.-M. *Chem. - Eur. J.* **2008**, *14*, 3013.
(45) George, G. N., EXAFSPAK, Stanford University: Stanford, CA, 2000.
(46) Neese, F. *WIREs Comput. Molec Sci.* **2012**, *2*, 73.
(47) Poiarkova, A. V.; Rehr, J. J. *Phys. Rev. B: Condens. Matter Mater. Phys.* **1999**, *59*, 948.
(48) Petrenko, T.; George, S. D.; Aliaga-Alcalde, N.; Bill, E.; Mienert, B.; Xiao, Y.; Guo, Y.; Sturhahn, W.; Cramer, S. P.; Wieghardt, K.; Neese, F. *J. Am. Chem. Soc.* **2007**, *129*, 11053.
(49) Roemelt, M.; Beckwith, M. A.; Duboc, C.; Collomb, M. N.; Neese, F.; DeBeer, S. *Inorg. Chem.* **2012**, *51*, 680.
(50) Becke, A. D. *Phys. Rev. A: At., Mol., Opt. Phys.* **1988**, *38*, 3098.
(51) Perdew, J. P. *Phys. Rev. B: Condens. Matter Mater. Phys.* **1986**, *33*, 8822.
(52) Lenthe, E. v.; Baerends, E. J.; Snijders, J. G. *J. Chem. Phys.* **1993**, *99*, 4597.
(53) van Wüllen, C. *J. Chem. Phys.* **1998**, *109*, 392.
(54) Pantazis, D. A.; Chen, X. Y.; Landis, C. R.; Neese, F. *J. Chem. Theory Comput.* **2008**, *4*, 908.
(55) Pantazis, D. A.; Neese, F. *WIREs Comput. Molec Sci.* **2014**, *4*, 363.
(56) Weigend, F.; Ahlrichs, R. *Phys. Chem. Chem. Phys.* **2005**, *7*, 3297.
(57) Klamt, A.; Schüürmann, G. *J. Chem. Soc., Perkin Trans. 2* **1993**, 799.
(58) Grimme, S. *J. Comput. Chem.* **2006**, *27*, 1787.
(59) Grimme, S. *J. Comput. Chem.* **2004**, *25*, 1463.
(60) Grimme, S.; Antony, J.; Ehrlich, S.; Krieg, H. *J. Chem. Phys.* 2010, *132*, 154104.
(61) Siegbahn, P. E. M. *J. Am. Chem. Soc.* **2009**, *131*, 18238.
(62) Grabolle, M.; Haumann, M.; Muller, C.; Liebisch, P.; Dau, H. *J. Biol. Chem.* **2006**, *281*, 4580.
(63) Galstyan, A.; Robertazzi, A.; Knapp, E. W. *J. Am. Chem. Soc.* **2012**, *134*, 7442.
(64) Laury, M. L.; Boesch, S. E.; Haken, I.; Sinha, P.; Wheeler, R. A.; Wilson, A. K. *J. Comput. Chem.* **2011**, *32*, 2339.
(65) Zhou, M. F.; Andrews, L.; Bauschlicher, C. W. *Chem. Rev.* **2001**, *101*, 1931.
(66) Ames, W.; Pantazis, D. A.; Krewald, V.; Cox, N.; Messinger, J.; Lubitz, W.; Neese, F. *J. Am. Chem. Soc.* **2011**, *133*, 19743.
(67) Pantazis, D. A.; Ames, W.; Cox, N.; Lubitz, W.; Neese, F. *Angew. Chem., Int. Ed.* **2012**, *51*, 9935.
(68) Askerka, M.; Vinyard, D. J.; Wang, J. M.; Brudvig, G. W.; Batista, V. S. *Biochemistry* **2015**, *54*, 1713.
(69) Krewald, V.; Retegan, M.; Cox, N.; Messinger, J.; Lubitz, W.; DeBeer, S.; Neese, F.; Pantazis, D. A. *Chem. Sci.* **2015**, *6*, 1676.
(70) Shoji, M.; Isobe, H.; Yamanaka, S.; Suga, M.; Akita, F.; Shen, J. R.; Yamaguchi, K. *Chem. Phys. Lett.* **2015**, *627*, 44.
(71) Hau-Riege, S. P.; Bennion, B. J. *Phys. Rev. E* 2015, *91*, 022705.
(72) van Schooneveld, M. M.; DeBeer, S. *J. Electron Spectrosc. Relat. Phenom.* **2015**, *198*, 31.
(73) Cox, N.; Pantazis, D. A.; Neese, F.; Lubitz, W. *Acc. Chem. Res.* **2013**, *46*, 1588.

DOI: 10.1021/jacs.5b00783
J. Am. Chem. Soc. 2015, 137, 12815−12834